

Modelling architected plate using a non-local derivative-free shear deformable plate theory

Mukul Saxena · Saikat Sarkar · J. N. Reddy

Received: 11 February 2023 / Accepted: 16 May 2023 / Published online: 14 July 2023 © Springer Nature B.V. 2023

Abstract The internal length scale relating to the cell size plays a crucial role in predicting the response of architected structures when subjected to external stimuli. A Volterra derivative-based approach for arriving at the non-local derivative-free continuum laws for architected structures is proposed. A mainstay of the work is the derivative-free directionality term, which recovers its classical counterpart in the infinitesimal limit. Using this approach, we derive the non-local integro-differential governing equations of a shear deformable plate. We also suggest a physical basis for the consideration of energy for nonaffine deformations and accurately estimate it by performing buckling analysis. This discards the requirement of the additional energy to be incorporated in an arbitrary manner for suppressing the unwanted spurious oscillations induced from zero energy modes. The numerical results demonstrate the efficacy of the proposed framework in precisely capturing the mechanical response of web-core shear deformable plate, thereby, manifesting the supremacy of the reduced model in shrinking the cost and computational time. To bolster our claim, various numerical models with different loading conditions have been analysed and compared against the three-dimensional FEM results.

Keywords Shear deformable plate · Nonlocal mechanics · derivative-free mechanics · Volterra derivative · Buckling analysis · Zero-energy mode

1 Introduction

From the body of a ship and bridge deck to biodegradable scaffolds in tissue engineering, architected materials are used in a wide range of applications. Due to their light weight and high strength to density ratio, architected materials (like web-core and lattice core panels) [1] have emerged as a potential alternative to various conventional materials. While conventional materials derive their properties from their chemical composition, architected materials gain majority of their properties from their architecture. For example, architecting different core shapes has enabled engineers to attain enhanced properties in the context of energy absorption capability [2], controllability of their elastic wave propagation, high stiffness to density ratio [3, 4], and vibration insulation characteristics. Such concept is also incorporated in designing structural members, like plates with periodic unit cell (e.g. sandwich panels). These unidirectional plates, specifically steel sandwich plates, have emerged as a promising alternative to buckling and

M. Saxena · S. Sarkar (⋈)

Department of Civil Engineering, Indian Institute of Technology Indore, Indore, Madhya Pradesh 453552, India

e-mail: saikat@iiti.ac.in

J. N. Reddy

Department of Mechanical Engineering, Texas A&M University, College Station, TX 77845, USA



bending load bearing structures. It has been claimed [5–7] that the steel sandwich panels offer 30–50% reduction in the weight of ship decks as compared to traditional stiffened steel plate models. Stiffened panels serve as the fundamental unit in composing the hull, deck and superstructure of ships. Steel sandwich panels have shown potential for their application in bridges and buildings [8-10]. Another application may be found in designing the space vehicles, in which the sandwich panels are used in designing light-weight load-bearing integrated thermal protection system (ITPS) [11]. One of the most common examples of architected materials is web-core panel, which consists of two flange sheets separated by a straight web sheet aligned orthogonally to the flange faces. The face sheets resist the bending and in-plane loads, while the inner core is designed for externally applied transverse load. Unfortunately, analysing such architected panels is computationally intensive and intractable when it comes to modelling the entire structure. Therefore, a computational model that preserves the structural information, without requiring detailed modeling of the unit cell, is fundamentally important for analyzing structures like ships, buildings, bridges etc. [12, 13]

In this regard, non-local continuum models [14, 15] may be good options since they can preserve such geometry information through their length-scale parameters. The works of Cosserat brothers [16] mark the earliest proposition of such generalized continuum theory, where each material point is assumed to possess a rotational degree of freedom (dof) in addition to its translational dof. Later-introduced non-local theories include Eringen's model involving higher order derivatives [17], variants of couplestress theory [18, 19] and modified couple stress theory [20, 21] (one may refer to [22] for detailed discussion on non-local elastic models). There are various applications of these nonlocal models (e.g. buckling and bending response of beams [23–25] and plates [26–28]).

Lately, equivalent single-layer (ESL) beam and plate models have been proposed for web-core sand-wich panels using classical couple stress [29], and micropolar [30, 31] continuum theories. These theories typically involve higher order derivatives [32] in the governing equations, which in general, are difficult to be handled within a finite element (FE)-based setup. Silling in 2000 introduced a theory named as

Peridynamics (PD) in which the evolution equations are a set of integro-differential equations, thus invoking the action at a distance rather than contact forces. Despite its well-posed structure in case of discontinuities, PD based framework experienced certain limitations like constrained Poisson's ratio (as in the case of bond based PD). Although this limitation has been relaxed through state based PD, yet arriving at the strictly PD based constitutive models is often difficult. This limitation can be bypassed by proposing a 'constitutive correspondence' between PD and the classical continuum mechanics (CCM) via nonlocalisation of the deformation gradient. But such an extension suffers from instability issues originating from the spurious zero-energy mode-induced oscillations. To surpass this issue, usually additional energy is provided in the form of spring stiffness, which may change the solution completely. Moreover, a priori estimation of this extra energy is another challenge.

In this study, we propose a non-local derivativefree continuum theory (DFCT) for precisely capturing the response of shear deformable plate with its application to steel sandwich panels in specific. The derivative-free governing equations are arrived at from the energy expression using Volterra derivative. The expression for derivative-free deformation gradient serves as the backbone of this study, which converges to the classical deformation gradient in the infinitesimal limit. Another key feature of this manuscript is the consideration of the energy corresponding to nonaffine deformations in a plate-like continuum, thereby, providing a physical basis for the addition of extra energy in an improvised manner for suppressing the zero-energy mode induced oscillations. The proposed model has a particular advantage in precisely capturing the deformations of architected materials where individual member may undergo localized deformation. Such localized deformations are difficult to be predicted in the traditional way. The efficacy of the proposed formalism is demonstrated by modelling an architected plate and comparing with the solution obtained from the detailed three-dimensional model. The results are also compared with 2D micropolar plate theory. The efficacy of the proposed model is validated by analysing the response for different loading and boundary conditions.

The rest of the paper is organised as follows. A derivative-free shear deformable plate model is proposed in Sect. 2. In Sect. 3, the governing equations



are arrived at from the energy expression by adopting Volterra derivative approach. Based on Navier's solution, different terms of governing equations are determined analytically in Sect. 4. Numerical models are solved for different loading conditions in Sect. 5. Imposition of pseudo boundary conditions is another key aspect of this section. This section also demonstrates the computation of additional energy term from the buckling response of the plate. Finally some concluding remarks are made in the Sect. 6.

2 Mathematical formulation

Let us consider an isotropic rectangular plate of side a and b, with uniform thickness h, placed along the Cartesian plane as shown in Fig. 1. Within the domain Ω , each material point X is assumed to interact non-locally with its neighbors Y, within an influence domain Ω_X , which is circle of finite radius r_c . The deformed locations of material points X and Y are denoted by X and Y respectively. The associated undeformed and deformed fiber lengths and fiber stretch are expressed as $r_{XY} := Y - X$, $r_{XY} := y - x$, $u_{XY} := r_{XY} - r_{XY}$.

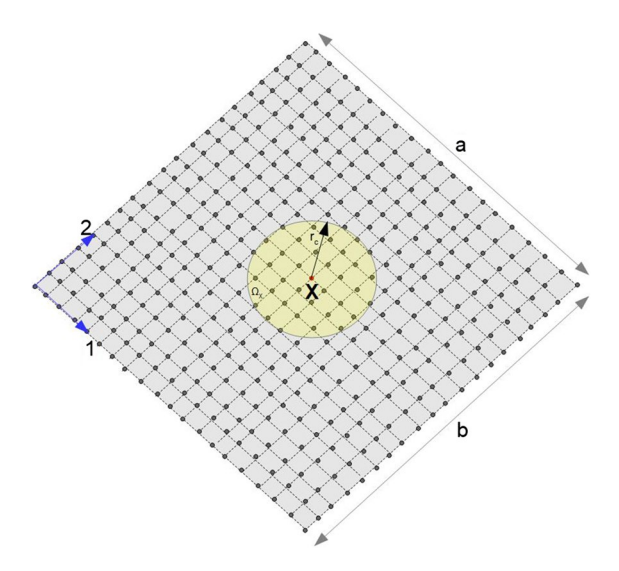


Fig. 1 Pictorial representation of a shear deformable plate

2.1 A nonlocal derivative free directionality term:

We begin with the derivation of an operator for a derivative-free nonlocal directionality term, $\hat{G}(u_3, X)$, which is used to relate an undeformed fiber with the associated stretch, $u_{XY} := \{(u_1)_{XY}, (u_2)_{XY}, (u_3)_{XY}\}$ such that,

$$(u_3)_y - (u_3)_x = \hat{G}(u_3, X_d) ((Y)_d - (X)_d)$$
 where $d = 1, 2$

where d is the dimensionality and u_1, u_2, u_3 represent displacements along axes 1, 2, and 3, respectively. In this paper, we have adopted the derivative-free directionality term (for detailed derivation, one may refer to [33]) to estimate the deformation in the bond (y-x). The expression for the derivative-free deformation gradient \hat{G} is given below.

$$\begin{split} \hat{G}(u_3, X_d) &= \\ \left[\int_{\Omega_X} ((u_3)_y - (\overline{u}_3)_Y) ((Y)_d - (\overline{Y})_d)^T dY \right] \\ \left[\int_{\Omega_X} ((Y)_d - (\overline{Y})_d) \left((Y)_d - (\overline{Y})_d \right)^T dY \right]^{-1} \end{split} \tag{2}$$

where (\bar{.}) represents the averaging operation over the domain Ω_X . The explicit expression mentioned in the above equation describes the non-local attribute of the proposed directionality term by considering faroff interactions. The proposed derivative-free directionality term approaches its classical counterpart in the infinitesimal limit (see "Appendix 1"). While the proposed directionality term operates on a finite influence domain like PD, they have certain differences. A comparative discussion between these two approaches is given in "Appendix 2". It may be interesting to note that a similar expression for the directionality term was arrived at in the context of optimization, particle filtering, upscaling and continuum mechanics using a sophisticated stochastic projection technique ([33–36]). The expression for \hat{G} has been proved to be the best estimator in L2P sense.

2.2 Displacement field

The shear deformable plate captures the deformation by the coupled effect of bending and shear displacements. In the deformed configuration, the



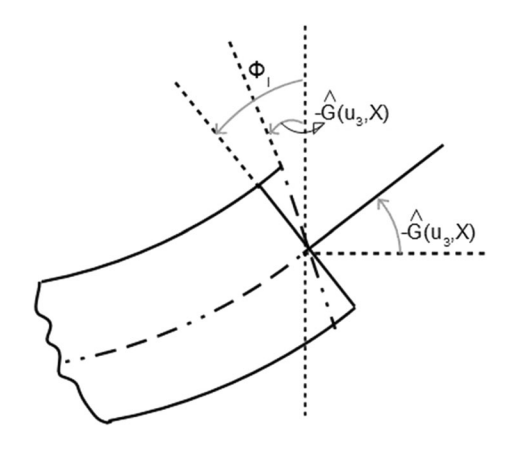


Fig. 2 Pictorial representation of a shear deformation at any cross-section in a shear deformable plate

rotations (θ_1, θ_2) about the plane normal to the neutral axes may be related to the transverse deformation u_3 and shear deformations (Φ_1, Φ_2) through the equations below (see Fig. 2):

$$\begin{aligned} -\theta_1 &= \hat{G}(u_3, X_1) + \Phi_1 \\ -\theta_2 &= \hat{G}(u_3, X_2) + \Phi_2 \end{aligned} \tag{3}$$

The 3D displacement of a plate may be approximated using the 2D displacements of the mid-surface kinematic variables, by recalling the inextensibility assumptions of the shear deformable plate. Thus, the displacement field of a material point at a distance z from the neutral axes, may be characterized as [37]:

$$(u_1)_X \approx (u_1^0)_X + z\Phi_1$$

$$(u_2)_X \approx (u_2^0)_X + z\Phi_2$$

$$(u_3)_X = (u_3^0)_X$$
(4)

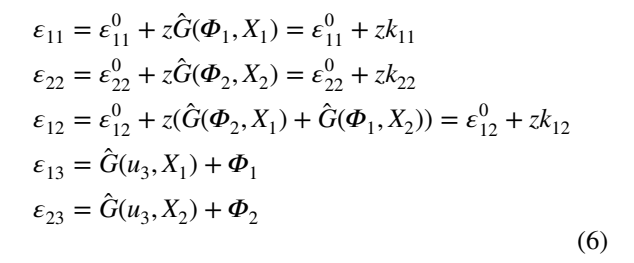
where (u_1^0, u_2^0) and u_3^0 denote the axial and transverse displacements respectively, at the neutral axis (i.e., at the plane z = 0). Accordingly, the velocity $\mathbf{v} := \{v_1, v_2, v_3\}$ of the material point \mathbf{X} takes the form:

$$v_{1} = (\dot{u}_{1})_{X} = (\dot{u}_{1}^{0})_{X} + z\dot{\Phi}_{1}$$

$$v_{2} = (\dot{u}_{2})_{X} = (\dot{u}_{2}^{0})_{X} + z\dot{\Phi}_{2}$$

$$v_{3} = (\dot{u}_{3})_{X} = (\dot{u}_{3}^{0})_{X}$$
(5)

with the non-zero strains as:



3 Governing equations

The Hamiltonian \mathcal{H} for the plate can be expressed as the sum total of the kinetic energy, \mathcal{K} and the potential energy Ψ .

$$\mathcal{H} = \mathcal{K} + \Psi \tag{7}$$

For any material point X having momentum p and mass density ρ , the kinetic energy (\mathcal{K}) may be expressed in the continuum limits as:

$$\mathcal{K} = \int_{\Omega} \frac{p \cdot p}{2\rho} d\Omega$$

$$\mathcal{K} = \int_{0}^{a} \int_{0}^{b} \int_{-h/2}^{h/2} \frac{\rho}{2} (((\dot{u}_{1}^{0})_{X} + z\dot{\theta}_{1})^{2} + ((\dot{u}_{2}^{0})_{X} + z\dot{\theta}_{2})^{2} + (\dot{u}_{3}^{0})_{X}^{2}) dz dX_{2} dX_{1}$$
(8)

The total potential energy (Ψ) for the nonaffine deformation of the plate may be expressed as the sum total of the potential energy due to axial stretching (Ψ_A) , shear deformation (Ψ_S) , nonlocal bending deformation (Ψ_{NLB}) (see Fig. 3), work done by externally applied transverse load q acting per unit area of the plate (Ψ_q) and the work done by in-plane loads N_{11} and N_{22} . This can be mathematically written as:

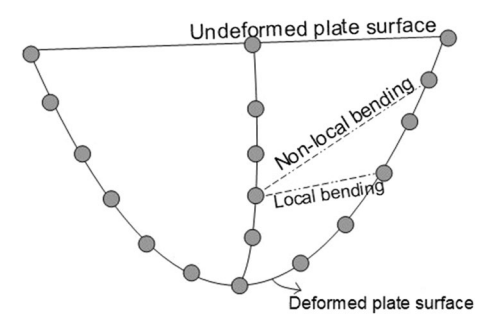


Fig. 3 Pictorial representation of non-local bending in a shear deformable plate



$$\Psi = \Psi_A + \Psi_S + \Psi_{NLB} - \Psi_q - \Psi_N$$

(9)

where E and μ represents the Young's modulus of elasticity and Poisson's ratio, respectively.

$$\Psi = \frac{1}{2} \int_{0}^{a} \int_{0}^{b} \int_{-h/2}^{h/2} \left[\sigma_{11} \varepsilon_{11} + \sigma_{22} \varepsilon_{22} + \sigma_{12} \varepsilon_{12} + \sigma_{31} \varepsilon_{31} + \sigma_{23} \varepsilon_{23} \right] dz dX_{2} dX_{1}
+ \frac{1}{2} \int_{0}^{a} \int_{0}^{b} \frac{k}{|\Omega_{X}|} \int_{\Omega_{X}} \left((u_{3})_{Y} - (u_{3})_{X} \right)^{2} dY dX_{2} dX_{1} - \frac{1}{2} \int_{0}^{a} \int_{0}^{b} q u_{3}^{2} dX_{2} dX_{1}
- \frac{1}{2} \int_{0}^{a} \int_{0}^{b} \left[N_{11} \left(\hat{G}(u_{3}, X_{1}) \right)^{2} + N_{22} \left(\hat{G}(u_{3}, X_{2}) \right)^{2} \right] dX_{2} dX_{1}$$
(10)

The second term on the right hand side of Eq. (10) accounts for the nonaffine deformations arising from the non-local bending between two material points.

Substituting Eqs. (6) and (11) in Eq. (10) and integrating through the thickness of the plate, we arrive at:

$$\Psi = \frac{1}{2} \int_{0}^{a} \int_{0}^{b} \int_{-h/2}^{h/2} \frac{E}{1 - \mu^{2}} \left[\left(\varepsilon_{11} + \mu \varepsilon_{22} \right) \varepsilon_{11} + \left(\mu \varepsilon_{11} + \varepsilon_{22} \right) \varepsilon_{22} + \frac{1 - \mu}{2} \left(\varepsilon_{12}^{2} + \varepsilon_{31}^{2} + \varepsilon_{23}^{2} \right) \right] \\
dz dX_{2} dX_{1} \\
+ \frac{1}{2} \int_{0}^{a} \int_{0}^{b} \frac{k}{|\Omega_{X}|} \int_{\Omega_{X}} \left((u_{3})_{Y} - (u_{3})_{X} \right)^{2} dY dX_{2} dX_{1} - \frac{1}{2} \int_{0}^{a} \int_{0}^{b} q u_{3}^{2} dX_{2} dX_{1} \\
- \frac{1}{2} \int_{0}^{a} \int_{0}^{b} \left[N_{11} \left(\hat{G}(u_{3}, X_{1}) \right)^{2} + N_{22} \left(\hat{G}(u_{3}, X_{2}) \right)^{2} \right] dX_{2} dX_{1}$$
(12)

The variable k denotes the non-local interparticle bending stiffness along the direction of u_3 . Recalling the stress-strain relations of an isotropic plate:

where S denotes the shear modulus of elasticity. Using the relation $(u_3)_Y - (u_3)_X = [\hat{G}(u_3, X_1) \ \hat{G}(u_3, X_2)].[(Y_1 - X_1) \ (Y_2 - X_2)]^T$, Equation (12) can be written as:

$$\Psi = \frac{1}{2} \int_{0}^{a} \int_{0}^{b} \int_{-h/2}^{h/2} \frac{E}{1 - \mu^{2}} \left[\left(\varepsilon_{11} + \mu \varepsilon_{22} \right) \varepsilon_{11} + \left(\mu \varepsilon_{11} + \varepsilon_{22} \right) \varepsilon_{22} \right] + \mathcal{S} \left(\varepsilon_{12}^{2} + \varepsilon_{31}^{2} + \varepsilon_{23}^{2} \right) dz dX_{2} dX_{1}
+ \frac{1}{2} \int_{0}^{a} \int_{0}^{b} \frac{k}{|\Omega_{X}|} \int_{\Omega_{X}} \left(\left(\hat{G}(u_{3}, X_{1})(Y_{1} - X_{1}) \right)^{2} + \left(\hat{G}(u_{3}, X_{2})(Y_{2} - X_{2}) \right)^{2} \right) dY dX_{2} dX_{1}
- \frac{1}{2} \int_{0}^{a} \int_{0}^{b} q u_{3}^{2} dX_{2} dX_{1} - \frac{1}{2} \int_{0}^{a} \int_{0}^{b} \left[N_{11} \left(\hat{G}(u_{3}, X_{1}) \right)^{2} + N_{22} \left(\hat{G}(u_{3}, X_{2}) \right)^{2} \right] dX_{2} dX_{1} \tag{13}$$

$$\begin{cases}
\sigma_{11} \\
\sigma_{22} \\
\sigma_{12} \\
\sigma_{31} \\
\sigma_{23}
\end{cases} = \frac{E}{1 - \mu^{2}} \begin{bmatrix} 1 & \mu & 0 & 0 & 0 \\
\mu & 1 & 0 & 0 & 0 \\
0 & 0 & \frac{1-\mu}{2} & 0 & 0 \\
0 & 0 & 0 & \frac{1-\mu}{2} & 0 \\
0 & 0 & 0 & 0 & \frac{1-\mu}{2} \end{bmatrix} \begin{cases}
\varepsilon_{11} \\
\varepsilon_{22} \\
\varepsilon_{12} \\
\varepsilon_{31} \\
\varepsilon_{23}
\end{cases} \tag{11}$$

Replacing $(\vartheta_1, \vartheta_2) = \left(\frac{6kr_c^2}{64a^2}\right)$ (for a square plate of side length *a*) in the above Eq. (13), we obtain:



$$\Psi = \frac{1}{2} \int_{0}^{a} \int_{0}^{b} \int_{-h/2}^{h/2} \frac{E}{1 - \mu^{2}} \left[\left(\varepsilon_{11} + \mu \varepsilon_{22} \right) \varepsilon_{11} + \left(\mu \varepsilon_{11} + \varepsilon_{22} \right) \varepsilon_{22} \right] + \mathcal{S} \left(\varepsilon_{12}^{2} + \varepsilon_{31}^{2} + \varepsilon_{23}^{2} \right) dz dX_{2} dX_{1}
+ \frac{1}{2} \int_{0}^{a} \int_{0}^{b} \left(\hat{G}(u_{3}, X_{1}) \right)^{2} \vartheta_{1} dX_{2} dX_{1} + \frac{1}{2} \int_{0}^{a} \int_{0}^{b} \left(\hat{G}(u_{3}, X_{2}) \right)^{2} \vartheta_{2} dX_{2} dX_{1}
- \frac{1}{2} \int_{0}^{a} \int_{0}^{b} q u_{3}^{2} dX_{2} dX_{1} - \frac{1}{2} \int_{0}^{a} \int_{0}^{b} \left[N_{11} \left(\hat{G}(u_{3}, X_{1}) \right)^{2} + N_{22} \left(\hat{G}(u_{3}, X_{2}) \right)^{2} \right] dX_{2} dX_{1} \tag{14}$$

It is interesting to note that as the non-locality diminishes (i.e. $r_c \to 0$), the additional stiffness also diminishes to zero (i.e. $\theta \to 0$), Thus recovering the classical energy expression for the shear deformable plate. Following the expressions from Eq. (6) and substituting them in Eq. (12), we arrive at:

$$\dot{p}(\boldsymbol{\Phi}_1) = -\frac{\delta \boldsymbol{\Psi}}{\delta \boldsymbol{\Phi}_1}, \ \dot{p}(\boldsymbol{\Phi}_2) = -\frac{\delta \boldsymbol{\Phi}}{\delta \boldsymbol{\Phi}_2} \ and \ \dot{p}(u_3) = -\frac{\delta \boldsymbol{\Psi}}{\delta u_3}$$
(17)

$$\Psi = \frac{1}{2} \int_{0}^{a} \int_{0}^{b} \int_{-h/2}^{h/2} \frac{E}{1 - \mu^{2}} \left[\left(zk_{11} + \mu zk_{22} \right) zk_{11} + \left(\mu zk_{11} + zk_{22} \right) zk_{22} \right]
+ \mathcal{S} \left(z^{2}k_{12}^{2} + \left(\hat{G}(u_{3}, X_{1}) + \boldsymbol{\Phi}_{I} \right)^{2} + \left(\hat{G}(u_{3}, X_{2}) + \boldsymbol{\Phi}_{II} \right)^{2} \right) dz dX_{2} dX_{1}
+ \frac{1}{2} \int_{0}^{a} \int_{0}^{b} \left(\hat{G}(u_{3}, X_{1}) \right)^{2} \vartheta_{1} dX_{2} dX_{1} + \frac{1}{2} \int_{0}^{a} \int_{0}^{b} \left(\hat{G}(u_{3}, X_{2}) \right)^{2} \vartheta_{2} dX_{2} dX_{1}
- \frac{1}{2} \int_{0}^{a} \int_{0}^{b} q u_{3}^{2} dX_{2} dX_{1} - \frac{1}{2} \int_{0}^{a} \int_{0}^{b} \left[N_{11} \left(\hat{G}(u_{3}, X_{1}) \right)^{2} + N_{22} \left(\hat{G}(u_{3}, X_{2}) \right)^{2} \right] dX_{2} dX_{1}$$
(15)

Representing bending stiffness $D := \frac{Eh^3}{12(1-\mu^2)}$ and integrating the above Eq. (15) through the thickness of the plate h:

$$\Psi = \frac{1}{2} \int_{0}^{a} \int_{0}^{b} D\left[\left(\hat{G}(\boldsymbol{\Phi}_{1}, X_{1}) + \mu \hat{G}(\boldsymbol{\Phi}_{2}, X_{2})\right) \hat{G}(\boldsymbol{\Phi}_{1}, X_{1}) + \left(\mu \hat{G}(\boldsymbol{\Phi}_{1}, X_{1}) + \hat{G}(\boldsymbol{\Phi}_{2}, X_{2})\right) \hat{G}(\boldsymbol{\Phi}_{2}, X_{2})\right] \\
+ \mathcal{S} \frac{h^{3}}{12} k_{12}^{2} + \mathcal{S} h\left(\left(\hat{G}(u_{3}, X_{1}) + \boldsymbol{\Phi}_{I}\right)^{2} + \left(\hat{G}(u_{3}, X_{2}) + \boldsymbol{\Phi}_{II}\right)^{2}\right) dX_{2} dX_{1} \\
+ \frac{1}{2} \int_{0}^{a} \int_{0}^{b} \left(\hat{G}(u_{3}, X_{1})\right)^{2} \vartheta_{1} dX_{2} dX_{1} + \frac{1}{2} \int_{0}^{a} \int_{0}^{b} \left(\hat{G}(u_{3}, X_{2})\right)^{2} \vartheta_{2} dX_{2} dX_{1} \\
- \frac{1}{2} \int_{0}^{a} \int_{0}^{b} q u_{3}^{2} dX_{2} dX_{1} - \frac{1}{2} \int_{0}^{a} \int_{0}^{b} \left[N_{11} \left(\hat{G}(u_{3}, X_{1})\right)^{2} + N_{22} \left(\hat{G}(u_{3}, X_{2})\right)^{2}\right] dX_{2} dX_{1}$$
(16)

Using the Volterra derivative as in ([38]), the governing equation of motions for the elastodynamic continuum are given by:



From Eq. (17), it can be computed that:

$$\begin{split} \dot{p}(\mathbf{\Phi}_{1}) &= \rho \frac{h^{3}}{12} \ddot{\mathbf{\Phi}}_{1} \\ \dot{p}(\mathbf{\Phi}_{2}) &= \rho \frac{h^{3}}{12} \ddot{\mathbf{\Phi}}_{2} \\ \dot{p}(u_{3}) &= \rho h \ddot{u}_{3} \\ \frac{\delta \Psi}{\delta \mathbf{\Phi}_{1}} &= D \hat{G}(\hat{G}(\mathbf{\Phi}_{1}, X_{1}), X_{1}) + D \mu \hat{G}(\hat{G}(\mathbf{\Phi}_{2}, X_{1}), X_{2}) \\ &+ \frac{S h^{3}}{12} \left(\hat{G}(\hat{G}(\mathbf{\Phi}_{1}, X_{2}), X_{2}) + \hat{G}(\hat{G}(\mathbf{\Phi}_{2}, X_{2}), X_{1}) \right) - S h \left(\hat{G}(u_{3}, X_{1}) + \mathbf{\Phi}_{1} \right) \\ \frac{\delta \Psi}{\delta \mathbf{\Phi}_{2}} &= D \hat{G}(\hat{G}(\mathbf{\Phi}_{2}, X_{2}), X_{2}) + D \mu \hat{G}(\hat{G}(\mathbf{\Phi}_{1}, X_{1}), X_{2}) \\ &+ \frac{S h^{3}}{12} \left(\hat{G}(\hat{G}(\mathbf{\Phi}_{2}, X_{1}), X_{1}) + \hat{G}(\hat{G}(\mathbf{\Phi}_{1}, X_{2}), X_{1}) \right) - S h \left(\hat{G}(u_{3}, X_{2}) + \mathbf{\Phi}_{2} \right) \\ \frac{\delta \Psi}{\delta u_{3}} &= S h \left(\hat{G}(\hat{G}(u_{3}, X_{1}), X_{1}) + \hat{G}(\mathbf{\Phi}_{1}, X_{1}) \right) + S h \left(\hat{G}(\hat{G}(u_{3}, X_{2}), X_{2}) + \hat{G}(\mathbf{\Phi}_{2}, X_{2}) \right) \\ &+ (N_{11} + \vartheta_{1}) \hat{G}(\hat{G}(u_{3}, X_{1}), X_{1}) + (N_{22} + \vartheta_{2}) \hat{G}(\hat{G}(u_{3}, X_{2}), X_{2}) - q \end{split}$$

Assuming that the transverse shear strains and corresponding shear stresses are constant throughout the thickness is fallacious. Therefore, to compensate for the discrepancy involved in the solution, a shear correction factor (k_s) is introduced in the above equations. Finally, the non-local derivative-free governing equations for a shear deformable plate takes the form:

deformable plate equations in the infinitesimal limit [39, 40]. One may also note that the derivative-free shear deformable plate theory recovers a derivative-free shear-rigid (Kirchhoff) plate theory for a thin plate (a discussion on this is given in "Appendix 3").

$$\rho \frac{h^{3}}{12} \ddot{\boldsymbol{\Phi}}_{1} = D\hat{G}(\hat{G}(\boldsymbol{\Phi}_{1}, X_{1}), X_{1}) + D\mu \hat{G}(\hat{G}(\boldsymbol{\Phi}_{2}, X_{1}), X_{2})$$

$$+ \frac{Sh^{3}}{12} \left(\hat{G}(\hat{G}(\boldsymbol{\Phi}_{1}, X_{2}), X_{2}) + \hat{G}(\hat{G}(\boldsymbol{\Phi}_{2}, X_{2}), X_{1}) \right) - k_{s}Sh(\hat{G}(u_{3}, X_{1}) + \boldsymbol{\Phi}_{1})$$

$$\rho \frac{h^{3}}{12} \ddot{\boldsymbol{\Phi}}_{2} = D\hat{G}(\hat{G}(\boldsymbol{\Phi}_{2}, X_{2}), X_{2}) + D\mu \hat{G}(\hat{G}(\boldsymbol{\Phi}_{1}, X_{1}), X_{2})$$

$$+ \frac{Sh^{3}}{12} \left(\hat{G}(\hat{G}(\boldsymbol{\Phi}_{2}, X_{1}), X_{1}) + \hat{G}(\hat{G}(\boldsymbol{\Phi}_{1}, X_{2}), X_{1}) \right) - k_{s}Sh(\hat{G}(u_{3}, X_{2}) + \boldsymbol{\Phi}_{2})$$

$$\rho h \ddot{u}_{3} = k_{s}Sh(\hat{G}(\hat{G}(u_{3}, X_{1}), X_{1}) + \hat{G}(\boldsymbol{\Phi}_{1}, X_{1})) + k_{s}Sh(\hat{G}(\hat{G}(u_{3}, X_{2}), X_{2}) + \hat{G}(\boldsymbol{\Phi}_{2}, X_{2}))$$

$$+ (N_{11} + \vartheta_{1})\hat{G}(\hat{G}(u_{3}, X_{1}), X_{1}) + (N_{22} + \vartheta_{2})\hat{G}(\hat{G}(u_{3}, X_{2}), X_{2}) - q$$

$$(19)$$

As the directionality term converges to its classical counterpart in an infinitesimal limit, the governing equations also converge to the classical shear

4 Navier's solution for bending and buckling

The analytical solution for the simply supported plate can be obtained by adopting the Navier's solution. The displacement fields are assumed as [31]:



$$u_{3} = \sum_{n=1}^{\infty} \sum_{m=1}^{\infty} (u_{3})_{mn} \sin(\alpha X_{1}) \sin(\beta X_{2})$$

$$\boldsymbol{\Phi}_{1} = \sum_{n=1}^{\infty} \sum_{m=1}^{\infty} (\boldsymbol{\Phi}_{1})_{mn} \cos(\alpha X_{1}) \sin(\beta X_{2})$$

$$\boldsymbol{\Phi}_{2} = \sum_{n=1}^{\infty} \sum_{m=1}^{\infty} (\boldsymbol{\Phi}_{2})_{mn} \sin(\alpha X_{1}) \cos(\beta X_{2})$$

$$q = \sum_{n=1}^{\infty} \sum_{m=1}^{\infty} Q_{mn} \sin(\alpha X_{1}) \sin(\beta X_{2})$$
(20)

where.

$$\alpha = \frac{m\pi}{a}$$

$$\beta = \frac{n\pi}{b}$$
(21)

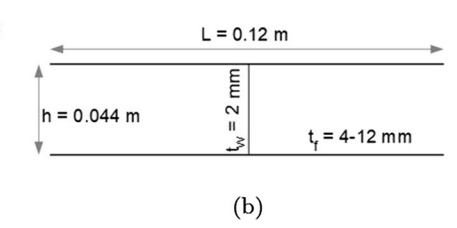
For the assumed displacement fields, the terms in Eq. (19) may be analytically computed for a finite radius of influence (r_c) (refer to "Appendix 4"):

$$\begin{split} \hat{G}(\hat{G}(\boldsymbol{\Phi}_{1},X_{1}),X_{1}) &= -C_{1}^{2}(\boldsymbol{\Phi}_{1})_{mn}\cos(\alpha X_{1})\sin(\beta X_{2}) \\ \hat{G}(\hat{G}(\boldsymbol{\Phi}_{1},X_{2}),X_{2}) &= -C_{2}^{2}(\boldsymbol{\Phi}_{1})_{mn}\cos(\alpha X_{1})\sin(\beta X_{2}) \\ \hat{G}(\hat{G}(\boldsymbol{\Phi}_{2},X_{1}),X_{1}) &= -C_{1}^{2}(\boldsymbol{\Phi}_{2})_{mn}\sin(\alpha X_{1})\cos(\beta X_{2}) \\ \hat{G}(\hat{G}(\boldsymbol{\Phi}_{2},X_{2}),X_{2}) &= -C_{2}^{2}(\boldsymbol{\Phi}_{2})_{mn}\sin(\alpha X_{1})\cos(\beta X_{2}) \\ \hat{G}(\hat{G}(\boldsymbol{\Phi}_{1},X_{1}),X_{2}) &= -C_{1}C_{2}(\boldsymbol{\Phi}_{1})_{mn}\sin(\alpha X_{1})\cos(\beta X_{2}) \\ \hat{G}(\hat{G}(\boldsymbol{\Phi}_{2},X_{1}),X_{2}) &= -C_{1}C_{2}(\boldsymbol{\Phi}_{2})_{mn}\cos(\alpha X_{1})\sin(\beta X_{2}) \\ \hat{G}(\hat{G}(u_{3},X_{1}),X_{1}) &= -C_{1}^{2}(u_{3})_{mn}\sin(\alpha X_{1})\sin(\beta X_{2}) \\ \hat{G}(\hat{G}(u_{3},X_{2}),X_{2}) &= -C_{2}^{2}(u_{3})_{mn}\sin(\alpha X_{1})\sin(\beta X_{2}) \\ \hat{G}(u_{3},X_{1}) &= -C_{1}(u_{3})_{mn}\cos(\alpha X_{1})\sin(\beta X_{2}) \\ \hat{G}(u_{3},X_{2}) &= -C_{2}(u_{3})_{mn}\sin(\alpha X_{1})\cos(\beta X_{2}) \\ \hat{G}(\boldsymbol{\Phi}_{1},X_{1}) &= C_{1}(\boldsymbol{\Phi}_{1})_{mn}\sin(\alpha X_{1})\sin(\beta X_{2}) \\ \hat{G}(\boldsymbol{\Phi}_{2},X_{2}) &= C_{2}(\boldsymbol{\Phi}_{2})_{mn}\sin(\alpha X_{2})\sin(\beta X_{2}) \\ \hat{G}(\boldsymbol{\Phi}_{2},X_{2}) &= C_{2}(\boldsymbol{\Phi}_{2})_{mn}\sin(\alpha X_$$

Fig. 4 A pictorial representation of **a** undeformed

web-core shear deformable plate and **b** specification of

its microstructural unit cell



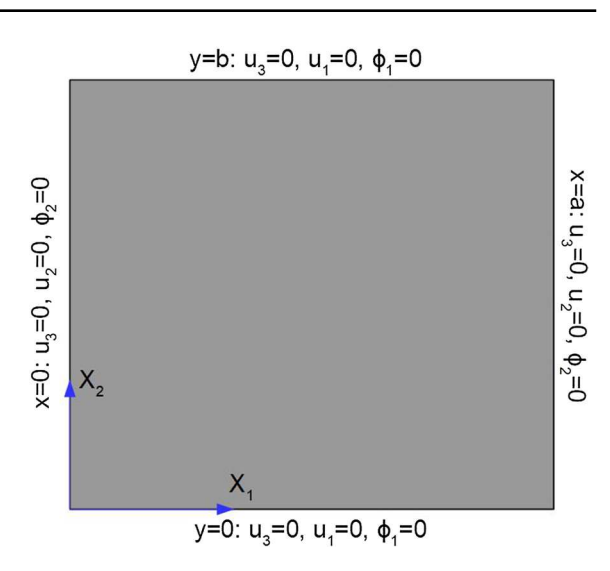


Fig. 5 Boundary conditions for buckling analysis of a simply supported shear deformable plate

$$C_1 = \frac{3}{\alpha^2 r_c^3} (\alpha r_c \cos(\alpha r_c) - \sin(\alpha r_c))$$

$$C_2 = \frac{3}{\beta^2 r_c^3} (\beta r_c \cos(\beta r_c) - \sin(\beta r_c))$$
(23)

Substitution of Eq. (22) into Eq. (19) yields the following relations for the coefficients $((u_3)_{mn}, (\Phi_1)_{mn}, (\Phi_2)_{mn}, Q_{mn})$ [41]:

$$\hat{M}\ddot{w} + \hat{k}w = Q \tag{24}$$

where,

$$w = \{(u_3)_{mn} (\boldsymbol{\Phi}_1)_{mn} (\boldsymbol{\Phi}_2)_{mn}\}^T$$

$$Q = \{Q_{mn} \ 0 \ 0\}^T$$
(25)

and

$$\hat{k} = \begin{bmatrix} \hat{k}_{11} & \hat{k}_{12} & \hat{k}_{13} \\ \hat{k}_{21} & \hat{k}_{22} & \hat{k}_{23} \\ \hat{k}_{31} & \hat{k}_{32} & \hat{k}_{33} \end{bmatrix}$$
 (26)



where.

$$\begin{split} \hat{k}_{11} &= -C_1^2 (k_s \beta h + N_{11} + \vartheta_1) - C_2^2 (k_s \beta h + N_{22} + \vartheta_2) \\ \hat{k}_{12} &= \hat{k}_{21} = C_1 k_s \beta h \\ \hat{k}_{13} &= \hat{k}_{31} = C_2 k_s \beta h \\ \hat{k}_{22} &= -C_1^2 D - C_2^2 \beta \frac{h^3}{12} - k_s \beta h \\ \hat{k}_{23} &= \hat{k}_{32} = -\mu D C_1 C_2 - C_1 C_2 \beta \frac{h^3}{12} \\ \hat{k}_{33} &= -C_1^2 \beta \frac{h^3}{12} - C_2^2 D - k_s \beta h \end{split}$$

For performing the buckling analysis, the in-plane biaxial compressive loads are applied through Eq. (27) as given below:

$$N_{11} = -fN_0, \ N_{22} = -N_0$$

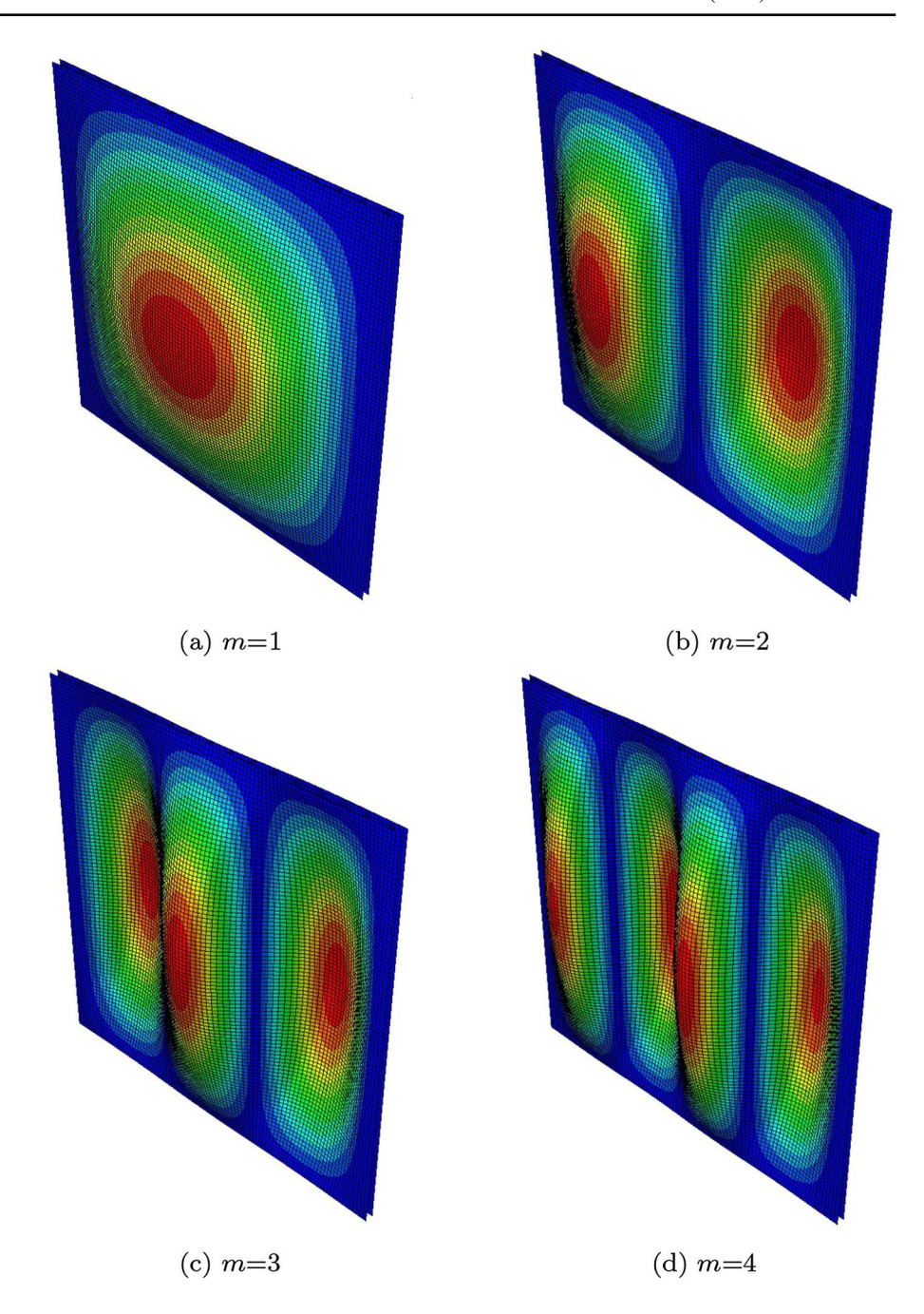
$$\theta_1 = f\theta_0, \ \theta_2 = \theta_0$$
(28)

where $f = N_{11}/N_{22}$. To obtain a non-trivial solution, the determinant of the \hat{k} matrix must be zero. This gives the following expression for the additional term θ_0 :

$$\begin{split} \vartheta_0 &= \frac{\mathcal{N}}{D} \\ \mathcal{N} &= D^2 N_0 C_1^2 C_2^4 + (\beta^3 C_1^2 C_2^2 h^5 k_s^2)/3 + D^2 N_0 C_1^4 C_2^3 f + (D\beta^2 C_1^6 h^4 k_s)/12 \\ &+ (D\beta^2 C_2^6 h^4 k_s)/12 + (N_0 \beta^2 C_2^4 h^4 k_s)/12 + D\beta^2 C_1^4 h^2 k_s^2 \\ &+ D\beta^2 C_2^4 h^2 k_s^2 - D^2 N_0 C_1^2 C_2^4 \mu^2 + N_0 \beta^2 C_2^2 h^2 k_s^2 \\ &+ (DN_0 \beta C_2^6 h^3)/12 + (D\beta^2 C_1^2 C_2^4 h^4 k_s)/12 + (D\beta^2 C_1^4 C_2^2 h^4 k_s)/12 \\ &- D^2 N_0 C_1^4 C_2^2 f \mu^2 + (N_0 \beta^2 C_1^2 C_2^4 h^4 k_s)/12 + (D\beta^2 C_1^4 C_2^2 h^3 k_s)/12 \\ &+ N_0 \beta^2 C_1^2 f h^2 k_s^2 + (DN_0 \beta C_1^6 h^3)/12 + (DN_0 \beta C_1^4 C_2^2 h^3 k_s)/12 \\ &+ N_0 \beta^2 C_1^2 f h^2 k_s + D^2 \beta C_1^4 C_2^2 h k_s + (N_0 \beta^2 C_1^4 f h^4 k_s)/12 \\ &+ D^2 \beta C_1^2 C_2^4 h k_s + D^2 \beta C_1^4 C_2^2 h k_s + (N_0 \beta^2 C_1^4 f h^4 k_s)/12 \\ &+ DN_0 \beta C_2^4 h k_s - (DN_0 \beta C_1^2 C_2^4 h^3 v)/6 + DN_0 \beta C_1^4 f h k_s \\ &+ (N_0 \beta^2 C_1^2 C_2^2 f h^4 k_s)/12 - D^2 \beta C_1^2 C_2^4 h k_s v^2 - D^2 \beta C_1^4 C_2^2 h k_s v^2 \\ &- (D\beta^2 C_1^2 C_2^4 h^4 k_s)/6 - (D\beta^2 C_1^4 C_2^2 f h^4 k_s)/6 \\ &+ DN_0 \beta C_1^2 C_2^4 h^3 y)/12 + DN_0 \beta C_1^2 C_2^4 h^4 k_s)/12 - D^2 C_1^2 C_2^4 v^2 + \beta^2 C_2^2 h^2 k_s^2 \\ &+ (D\beta C_0^2 h^3)/12 + D\beta C_1^2 h k_s / 12 - D^2 C_1^2 C_2^4 v^2 + \beta^2 C_2^2 h^2 k_s^2 \\ &+ (D\beta C_0^2 h^3)/12 + D\beta C_1^2 (h^4 k_s)/12 - D^2 C_1^2 C_2^4 v^2 + \beta^2 C_2^2 h^2 k_s^2 \\ &- D^2 C_1^4 C_2^2 h^2 + (\beta^2 C_1^2 C_2^4 h^4 k_s)/12 - D^2 C_1^2 C_2^4 v^2 + \beta^2 C_2^2 h^2 k_s^2 \\ &+ (D\beta C_0^4 h^3)/12 + D\beta C_1^2 C_1^4 h^4 k_s)/12 \\ &+ (D\beta C_1^4 C_2^3 h^3)/12 - (D\beta C_1^2 C_2^4 h^3 k_s)/12 + D\beta C_1^4 C_2^4 h^3 k_s)/12 + D\beta C_1^2 C_2^4 h^4 k_s)/12 \\ &+ (D\beta C_1^2 C_2^4 h^4 k_s)/12 + D\beta C_1^2 C_2^4 h^4 k_s)/12 \\ &+ (D\beta C_1^2 C_2^4 h^4 k_s)/12 + D\beta C_1^2 C_2^4 h^3 k_s)/12 \\ &+ (D\beta C_1^2 C_2^3 h^4 k_s)/12 + D\beta C_1^2 C_2^4 h^3 k_s)/12 \\ &+ (D\beta C_1^2 C_2^3 h^4 k_s)/12 + D\beta C_1^2 C_2^4 h^3 v)/6 \\ &+ D\beta C_1^2 C_2^3 h^4 k_s)/12 + D\beta C_1^2 C_2^4 h^3 v)/6 \\ &+ D\beta C_1^2 C_2^3 h^4 k_s / (D\beta C_1^4 C_2^3 h^3 v)/6) \end{split}$$



Fig. 6 Buckling analysis of a corrugated shear deformable plate with simply supported boundary conditions



5 Numerical simulation

As discussed in the previous section, the additional energy is derived from the buckling analysis of the structural member. Accordingly, we first study the buckling response of a web core plate with detailed modelling by considering two square plates with sides 2.04 m and 1.2 m each. The global element size

for each plate is taken as 24 mm. The shell elements, S8R5 (an 8-node doubly curved thick shell, reduced integration) are adopted for 3D FEM analysis using ABAQUS software. The microstructure of the plate is modelled by periodically repeating the unit cell geometry as shown in Fig. 4a. The dimensions of the unit cell are as follows: length of the unit cell L=0.12 m, height h=0.044 m, thickness of web $t_w=2$ mm, and



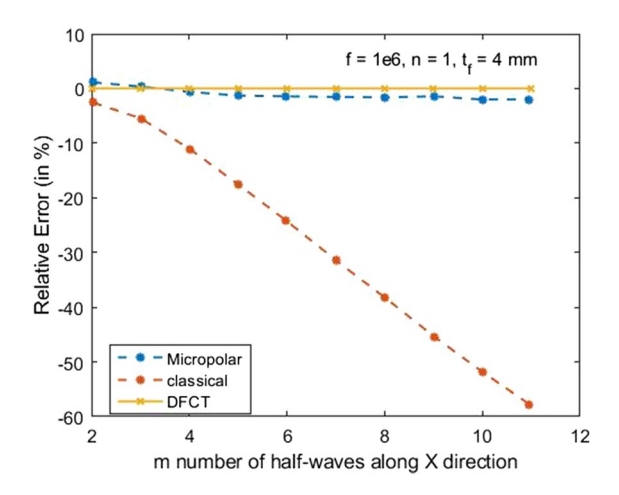


Fig. 7 Comparison of the relative percentage error obtained via different methodologies on performing the uniaxial buckling analysis of a shear deformable plate with corrugations

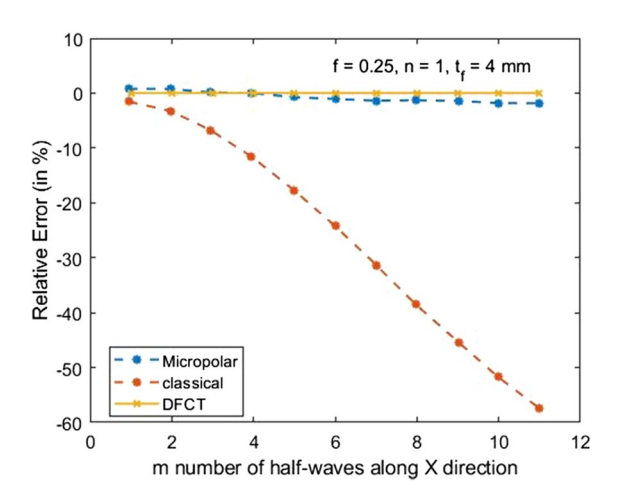


Fig. 8 Comparison of the relative percentage error obtained via different methodologies on performing the biaxial buckling analysis of a shear deformable plate with corrugations

thickness of flange t_f is varied from 4 mm to 12 mm. A pictorial representation of the unit cell specifications and the undeformed web-core shear deformable plate is presented through Fig. 4b.

The value of shear correction factor is taken as 5/6. As the value of $k_s = 5/6$ corresponds to a rectangular cross-section, an equivalent height of the plate is computed through the formula $h_e = 2t_f + t_w(h - 2t_f)$. Young's modulus and Poisson's ratio are assumed to be 206 GPa and 0.3, respectively. The density of material

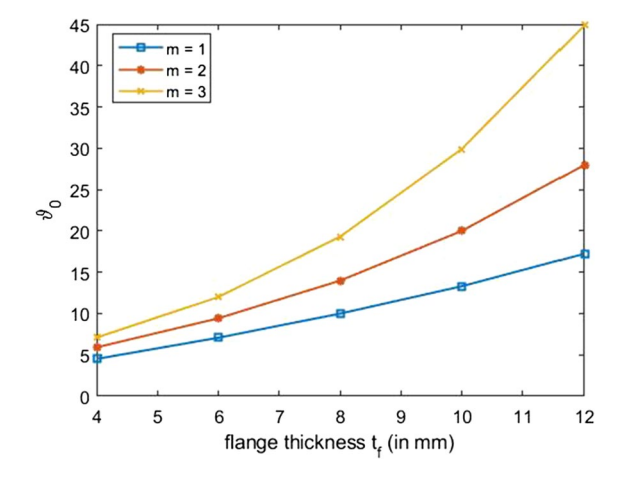


Fig. 9 Variation in the value of θ_0 on varying the thickness of flange in a corrugated shear deformable beam. (n=1, f=0.25)

is taken as $\rho = 7850 \text{ kg/m}^3$. For performing the buckling analysis, we set the time derivative terms and the transverse load to zero in Eq. (24). The buckling analysis is performed in two stages: first, for 'Stress perturbation' the conditions $u_3 = \Phi_2 = 0$ are set at x = 0 and x = a. After that, for the 'Buckling mode calculation' we set $u_3 = u_2 = \Phi_2 = 0$ at x = 0 and x = a. The pictorial representation of the same is given in Fig. 5.

Based on these boundary conditions, the buckling analysis of the corrugated plate is performed using 3D FEM. The value of f is taken sufficiently large (i.e. $f=10^6$) to demonstrate the uniaxial buckling while the value of f=0.25 is assumed to perform the biaxial buckling analysis of the corrugated plate. Various buckling modes for a shear deformable plate of size a=2.04 m are presented through Fig. 6. Corresponding buckling loads and additional energy terms are computed for each buckling mode.

The value of the number of half-waves, m, along 1 direction is varied from 2 to 11 and the buckling loads are computed through the proposed formalism for uniaxial and biaxial compressive loading. The results obtained via derivative-free framework are compared with the 2D micropolar and classical results (taken from [31]). The relative percentage error from the results via 3D FEM is computed and presented in Figs. 7 and 8. The error is computed through the following formula:



Fig. 10 Pictorial representation of square plate (blue dots) surrounded by pseudo boundary (red dots). (Color figure online)

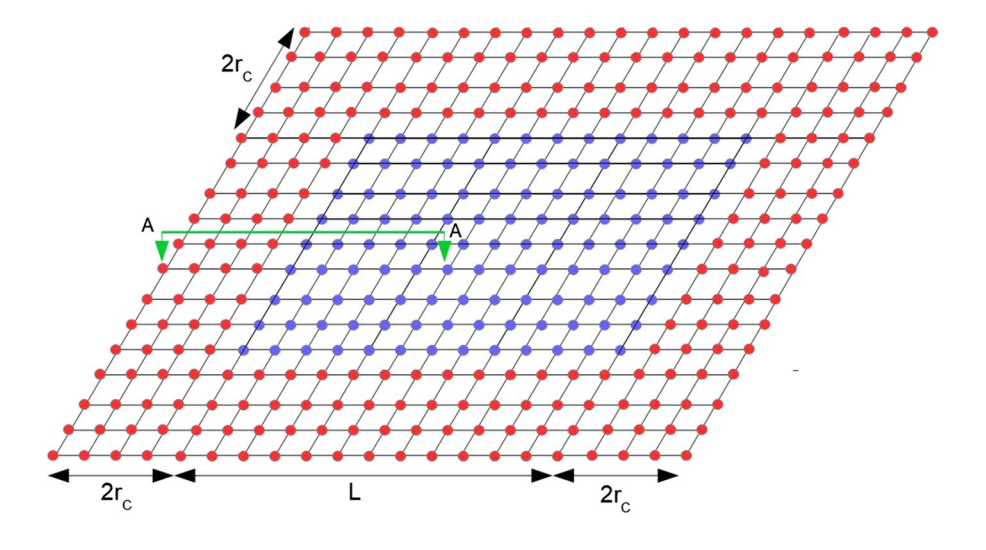
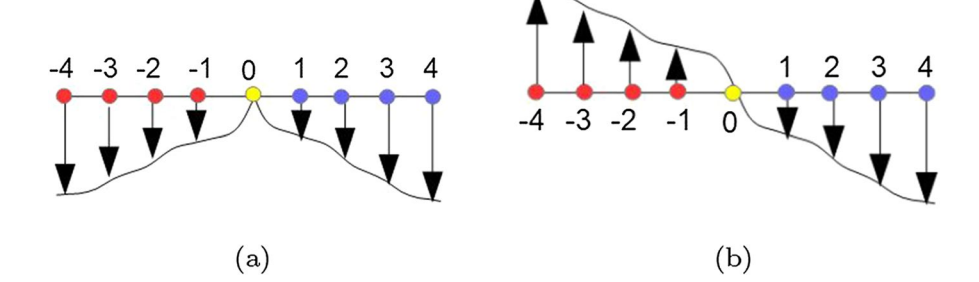


Fig. 11 Boundary effect minimization for a clamped b simply supported shear deformable plate



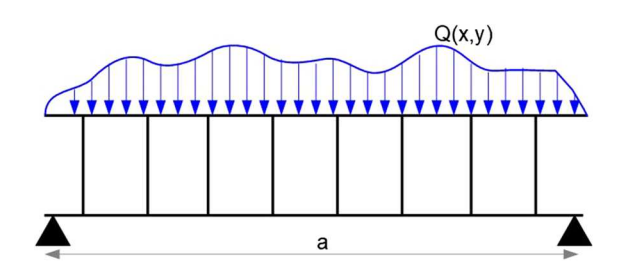


Fig. 12 Pictorial representation of a simply supported webcore plate subjected to externally applied load

$$Error = \frac{(N_0)_{\text{method}} - (N_0)_{3\text{DFEM}}}{(N_0)_{3\text{DFEM}}} \times 100$$
 (30)

We further examine the effect of varying the flange thickness on the additional energy term (ϑ_0) . For this purpose, different plates are modelled and buckling

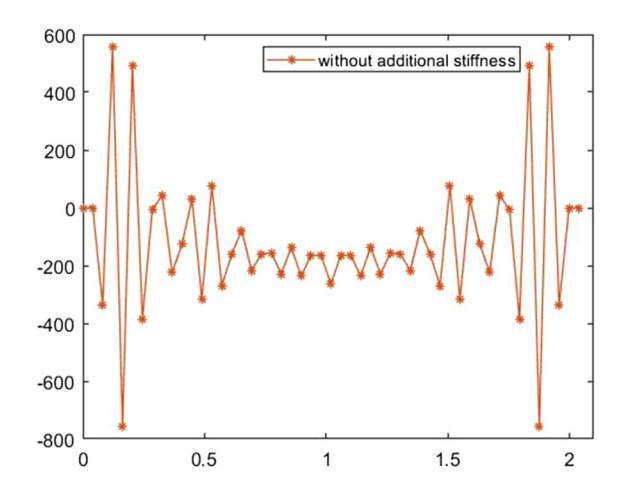


Fig. 13 The non-local transverse deformation in a simply supported web-core shear deformable plate without incorporating the additional energy term



loads are computed by varying the flange thickness from 4 to 12 mm. As the thickness of the flange increases, the corresponding buckling load also increases. Consequently, the value of θ_0 should also increase to satisfy the energy requirement. Similar trends have been recorded through proposed framework and the results are presented in Fig. 9.

Therefore, the non-local parameter can be estimated by performing the buckling analysis of the plate and incorporating the recorded buckling load in Eq. 29. The estimated non-local parameter efficiently removes the spurious zero-energy based oscillations and provides a stabilised solution, which is in good agreement with detailed 3D-FE simulation.

5.1 Imposition of boundary conditions on pseudo-nodes

One important aspect of the simulation is the imposition of the boundary conditions. We address this issue by incorporating pseudo nodes on each side of the plate. A fictitious region of length twice the radius of influence domain (r_c) is adopted on each side of the plate. A pictorial representation of the plate with pseudo nodes is presented in Fig. 10.

Different BCs are imposed as given below. Clamped BC:

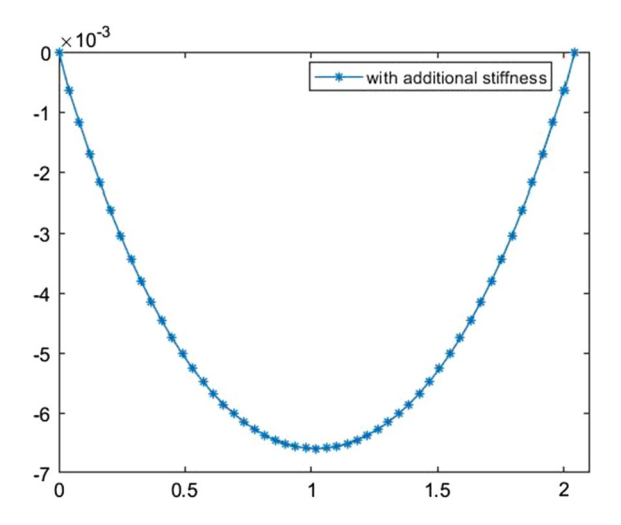


Fig. 14 The non-local transverse deformation in a simply supported web-core shear deformable plate after incorporating the additional energy term

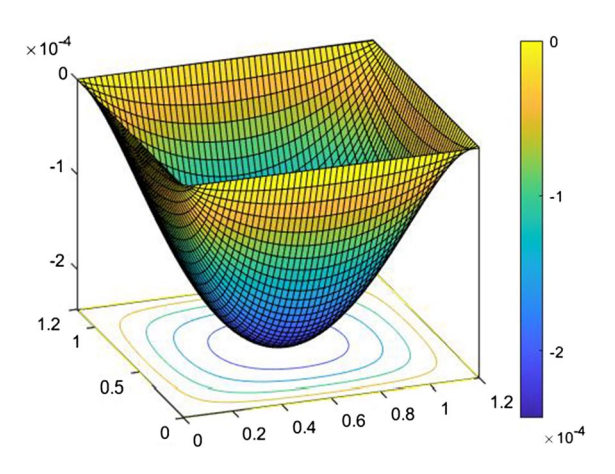


Fig. 15 The transverse deformation in a simply supported shear deformable plate under the application of uniformly distributed load

$$\begin{split} i)(u_3)_{-\mathcal{P}} &= (u_3)_{\mathcal{P}} & at \, x = (0,a) \, and \, y = (0,b) \\ ii)(\pmb{\Phi}_1)_{-\mathcal{P}} &= -(\pmb{\Phi}_1)_{\mathcal{P}} & at \, x = (0,a) \\ iii)(\pmb{\Phi}_2)_{-\mathcal{P}} &= -(\pmb{\Phi}_2)_{\mathcal{P}} & at \, y = (0,b) \end{split} \tag{31}$$

Simply Supported BC:

$$i)(u_3)_{-\mathcal{P}} = -(u_3)_{\mathcal{P}} \quad at \, x = (0, a) \, and \, y = (0, b)$$
 $ii)(\Phi_1)_{-\mathcal{P}} = (\Phi_1)_{\mathcal{P}} \quad at \, x = (0, a)$
 $iii)(\Phi_2)_{-\mathcal{P}} = (\Phi_2)_{\mathcal{P}} \quad at \, y = (0, b)$
(32)

The pictorial representation of the boundary conditions is presented in Fig. 11.

5.2 Static deformation in a Simply supported plate

We further examine a simply supported shear deformable plate under the application of a uniformly distributed load (see Fig. 12). For this purpose, we set the time derivative terms and the in-plane axial loads

Table 1 Comparison of the maximum transverse deformation obtained via different methodologies

S.No.	Methodology	Max. Transverse deformation	Relative % error
1.	3D FEM	0.2427	_
2.	DFCT	0.2425	-0.082
3.	2D Micropolar [31]	0.2449	0.906
4.	2D Classical [31]	0.2512	3.502



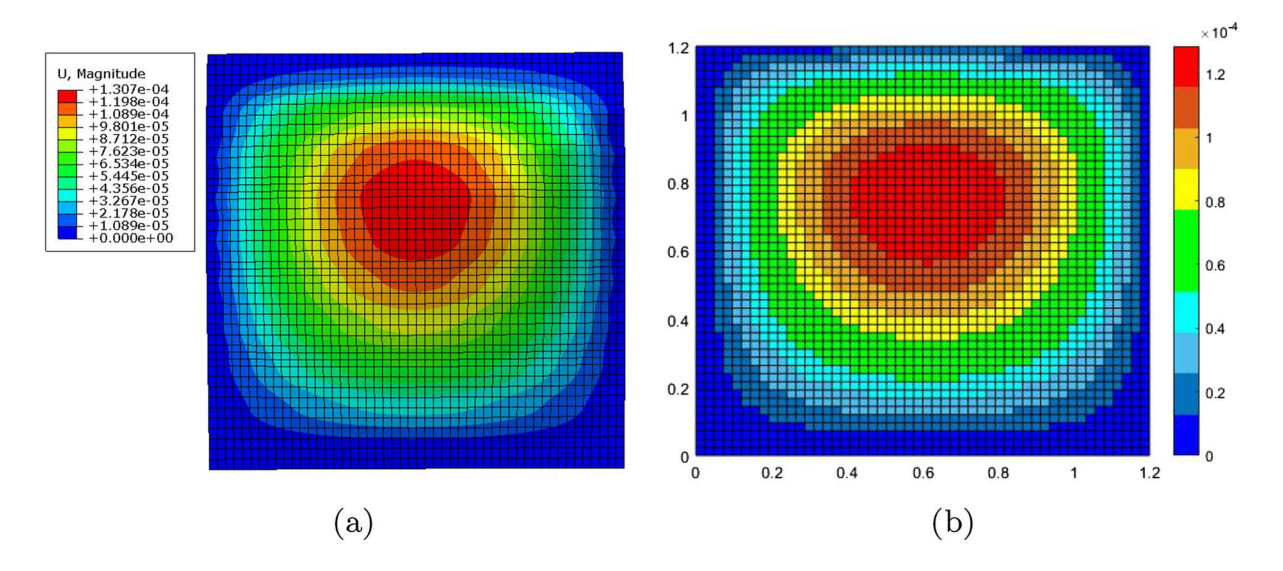


Fig. 16 Estimation of transverse deformation through a 3D FEM and b proposed framework for a simply supported shear deformable plate subjected uniformly varying load

to be zero. The derivative-free non-local governing equations are solved in their strong form. The plate of dimension 2.04×2.04 m² is modelled by adopting the same unit cell and material properties as discussed in the previous section.

The plate is discretized into 3481 nodes by uniformly distributing them at a spacing of $\Delta X = 24$ mm. The radius of influence (r_c) is taken as 52.3 mm,

which corresponds to approximately $2.18\Delta X$. A uniformly distributed load $Q_{mn}=16q_0/(\pi mn)$, where $q_0=10000$ N/m², is applied along the downward direction. We firstly examine the non-local response without the additional energy term. The model is observed to behave in an non-physical manner. The response of the middle section of the web-core plate is presented in Fig. 13.

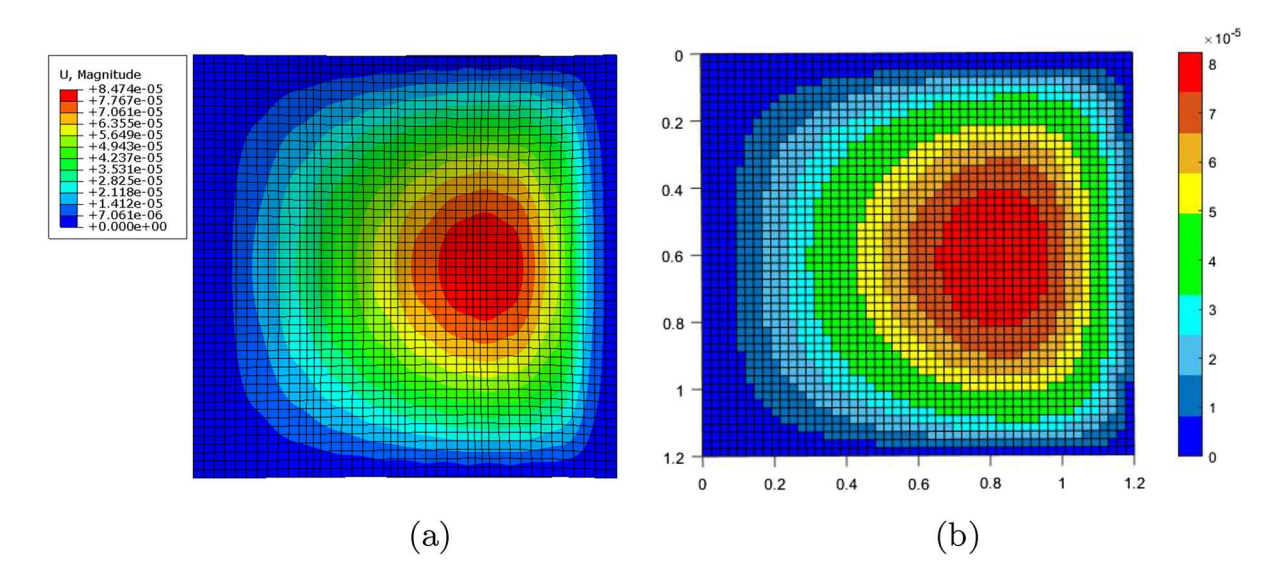


Fig. 17 Estimation of transverse deformation through a 3D FEM and b proposed framework for a simply supported shear deformable plate subjected parabolic load



These unphysical deformations are settled down by addition of the proposed extra energy term. To bolster our claim, we incorporate the additional extra energy term $\vartheta_0 = 22.962$ MN, which is obtained from the buckling analysis of the plate. The results obtained after the addition of extra energy term are found to be in accordance with the expected deformed shape of the plate. The transverse deformation of the mid section of the plate is presented in Fig. 14.

To examine the accuracy of the proposed model, we further study the response of a corrugated shear deformable plate with side a=1.2m. The plate is simply supported at all edges and the imposition of pseudo boundaries is implemented as discussed in the previous section. The thickness of the flange is taken as 6mm. The plate is subjected to a uniformly distributed load $Q_{mn} = 16q_0/(\pi mn)$, where $q_0 = 10000$ N/m². The additional energy term is incorporated and the transverse deformation of the mid plate section is recorded for m=2 and n=1. The transverse deformation in the plate is presented in Fig. 15.

The result is found to be in good agreement with the 3D FE result. The maximum transverse deformation of the mid section of the plate is recorded via 3D FEM, proposed model, 2D micropolar and 2D classical theory. The results for 2D micropolar and 2D classical theory have been taken from [31]). The relative percentage error is computed through the formula (Table 1).

$$\Delta(u_3) = \frac{(u_3)_{\text{method}} - (u_3)_{3\text{DFEM}}}{(u_3)_{3\text{DFEM}}} \times 100$$
 (33)

5.3 Static analysis of simply supported plate under the application of unsymmetrical loading condition

We extend our study to demonstrate the efficacy of the proposed framework in precisely capturing the response of the corrugated shear deformable plate under the application of unsymmetrical transverse loading conditions. The steel plate is modelled with the dimensions and material properties same as discussed above. The plate is discretised into 3481 particles uniformly spaced at an inter-particle distance of 24mm. The simply supported boundary conditions are imposed on all the sides on the plate. The pseudo boundaries are implemented as per the Eq. (32). We first examine the response of the plate under the application of uniformly varying load such that $Q_{mn}(x) = 16q_0/(\pi mn)(\frac{x}{a})$, where $q_0 = 10000$ N. The response is recorded and presented through Fig. 16. The corresponding 3D model is analysed using FEM software. The results obtained through proposed

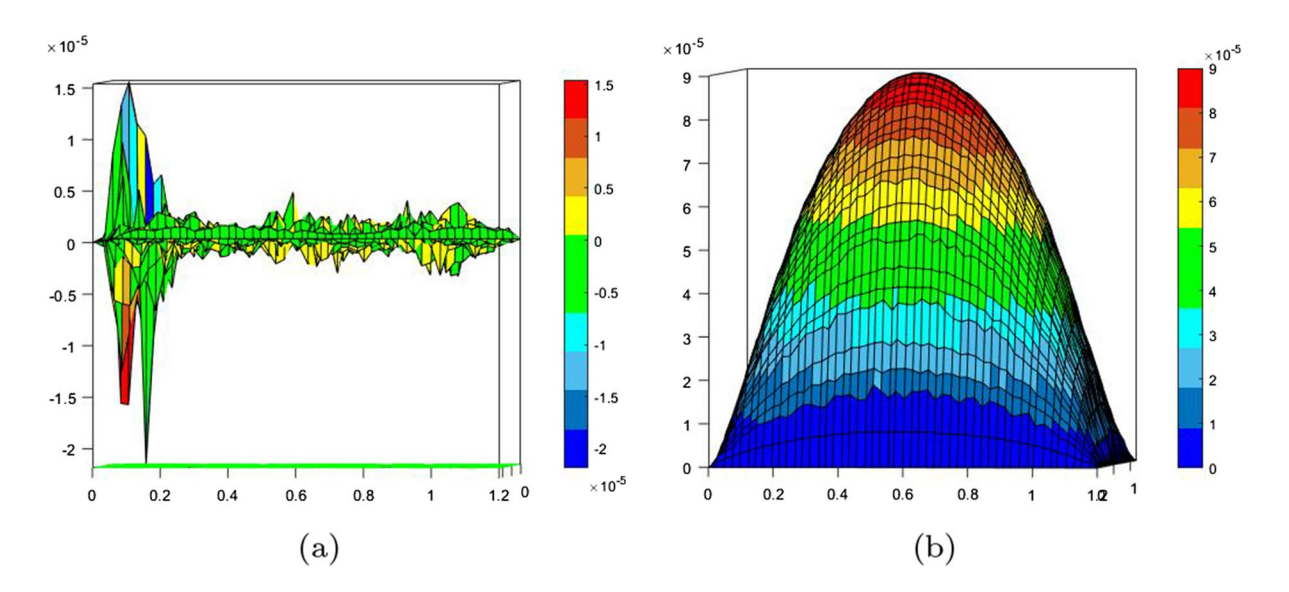


Fig. 18 Comparison of zero energy oscillations in simply supported shear deformable plate subjected to uniformly distributed load when analysed via (a) PD and (b) proposed method



framework are found in good agreement with the 3D FEM results.

To bolster our claim, we further examine the same plate under the application of parabolic loading such that $Q_{mn}(x) = 16q_0/(\pi mn)\left(\frac{x}{a}\right)^2$, where $q_0 = 10000$ N. The response is recorded and is presented through Fig. 17. The results obtained through proposed framework are found in good agreement with the 3D FEM results.

6 Conclusions

In this work, we have introduced a Volterra derivative based approach to arrive at the derivative-free non-local reduced dimensional continuum model. In specific, we have derived the integro-differential governing equations for a shear deformable plate. The equations have been derived from the nonaffine energy of the plate. The buckling analysis of the plate has been performed to determine the additional energy required for suppressing the zero-energy mode induced oscillations. The results obtained from the proposed framework are more accurate in predicting the transverse deformation of a corrugated plate, in comparison to the 2D classical and 2D micropolar theory. Various numerical exercises have been performed to showcase the efficacy of the proposed formalism in capturing the response of the architected plate under the application of different loading conditions.

The authors would like to extend the study in the future to derive the non-local reduced model for shell structures by considering the corresponding nonaffine energy expression.

Acknowledgements The authors acknowledge Professor Arun Srinivasa (Department of Mechanical Engineering, Texas A& M University, College Station, TX 77845, Unites States) for sharing his valuable comments and suggestions, which greatly improved the quality of the results included here.

Funding MS and SS acknowledge SERB (ECR/2018/001672) for supporting this work. JNR acknowledges the National Science Foundation (CMMI grant No. 1952873) for supporting this work.

Data availability The authors will make the data available on reasonable request.

Declarations

Competing interests The authors declare that there are no competing interests with publication of this work.

Appendix 1: Localization of derivative-free deformation gradient *G*

The proposed derivative-free directionality term approaches its classical deformation gradient counterpart in the infinitesimal limit. For demonstration, let us assume sufficient smoothness of the field such that the displacement (u_3) at a material point Y, in the neighbourhood of X, can be approximated using a truncated Taylor expansion as:

$$(u_3)_Y \approx (u_3)_X + \nabla(u_3, X_d)(Y_d - X_d),$$
 (34)

where ∇ is the classical gradient operator. The average stretch around X may also be approximated in a similar way.

$$(\bar{u}_3)_Y \approx (u_3)_X + \nabla(u_3, X_d)(\overline{Y_d - X_d}). \tag{35}$$

The nonlocal derivative-free deformation gradient is expressed as:

$$G(u_3, X_d) = I + \hat{G}(u_3, X_d)$$

$$= I + \left[\int_{\Omega_x} \left((u_3)_Y - (\bar{u}_3)_Y \right) \left(Y_d - \bar{Y}_d \right)^T dY \right]$$

$$\left[\int_{\Omega_x} \left(Y_d - \bar{Y}_d \right) \left(Y_d - \bar{Y}_d \right)^T dY \right]^{-1},$$
(36)

where I is the identity tensor. Replacing the terms in Eq. (36) with those given in Eqs. (34) and (35), we get,



$$G \approx I + \left[\int_{\Omega_{x}} \left((u_{3})_{X} + \nabla(u_{3}, X_{d})(Y_{d} - X_{d}) - ((u_{3})_{X} + \nabla(u_{3}, X_{d})(\overline{Y_{d}} - \overline{X_{d}})) \right) \left(Y_{d} - \overline{Y}_{d} \right)^{T} dY \right].$$

$$I + \left[\int_{\Omega_{x}} (Y_{d} - \overline{Y}_{d})(Y_{d} - \overline{Y}_{d})^{T} dY \right]^{-1}$$

$$= I + \left[\int_{\Omega_{x}} \nabla(u_{3}, X_{d})(Y_{d} - X_{d} - \overline{Y_{d}} - \overline{X_{d}}) \left(Y_{d} - \overline{Y}_{d} \right)^{T} dY \right] \left[\int_{\Omega_{x}} (Y_{d} - \overline{Y}_{d})(Y_{d} - \overline{Y}_{d})^{T} dY \right]^{-1}$$

$$= I + \nabla(u_{3}, X_{d}) \left[\int_{\Omega_{x}} (Y_{d} - X_{d} - \overline{Y}_{d}) \left(Y_{d} - \overline{Y}_{d} \right)^{T} dY \right] \left[\int_{\Omega_{x}} (Y_{d} - \overline{Y}_{d})(Y_{d} - \overline{Y}_{d})^{T} dY \right]^{-1}$$

$$= I + \nabla(u_{3}, X_{d}) \left[\int_{\Omega_{x}} (Y_{d} - \overline{Y}_{d}) \left(Y_{d} - \overline{Y}_{d} \right)^{T} dY \right] \left[\int_{\Omega_{x}} (Y_{d} - \overline{Y}_{d})^{T} dY \right]^{-1}$$

$$= I + \nabla(u_{3}, X_{d})$$

where F is the classical deformation gradient.

Appendix 2: Comparison of DFCT based non-local deformation gradient and PD based counterpart

The following non-local gradient term in the DFCT is actually rooted in measure theory and has been derived via a stochastic projection technique [33]. A similar expression may also be found in stochastic filtering [42, 43].

arrived at via constitutive correspondences using PD [47–49] and DFCT gradient terms. For simplicity, the material properties of the plate have been kept uniform and boundary conditions in the form of simple supports are considered at all the four sides of the plate. Under a uniform distribution of particles, the two approaches give the same solution. However, for random distribution, the PD variant exhibits unphysical oscillations, whereas the DFCT appears to work fine (see Fig 18).

$$\hat{G}_{DFCT}(u_3, X_d) = \left[\int_{\Omega_x} \left((u_3)_Y - (\bar{u}_3)_Y \right) \left(Y_d - \bar{Y}_d \right)^T dY \right] \left[\int_{\Omega_x} \left(Y_d - \bar{Y}_d \right) \left(Y_d - \bar{Y}_d \right)^T dY \right]^{-1}$$
(38)

On the other hand, the non-local gradient term for the PD correspondence may be written as [44-46]:

$$\hat{G}_{PD}(u_3, X_d) = \left[\int_{\Omega_x} \left((u_3)_Y - (u_3)_X \right) \left(Y_d - X_d \right)^T dY \right] \left[\int_{\Omega_x} \left(Y_d - X_d \right) \left(Y_d - X_d \right)^T dY \right]^{-1}$$
(39)

The above two expressions become identically same when $(u_3)_X$ and X_d , which is perhaps the case when there are detectable symmetries (e.g. through material homogeneity and/or symmetries in applied loading configurations). This is however not true in general and accordingly the two expressions differ. To numerically assess the performances of the two expressions, we have considered a shear deformable plate model,

Appendix 3: Equivalence of shear deformable plate theory and the shear-rigid plate theory in static case

Here we demonstrate that the derivative-free shear deformable plate theory is equivalent to shear-rigid (Kirchhoff) plate theory for a thin plate. The nonlocal governing equations for the shear deformable



plate subjected to transverse load q/unit area can be written as:

$$D\hat{G}(\hat{G}(\boldsymbol{\Phi}_{1}, X_{1}), X_{1}) + D\mu\hat{G}(\hat{G}(\boldsymbol{\Phi}_{2}, X_{1}), X_{2}) + \frac{Sh^{3}}{12} (\hat{G}(\hat{G}(\boldsymbol{\Phi}_{1}, X_{2}), X_{2}) + \hat{G}(\hat{G}(\boldsymbol{\Phi}_{2}, X_{2}), X_{1})) - k_{s}Sh(\hat{G}(u_{3}, X_{1}) + \boldsymbol{\Phi}_{1}) = 0$$

$$(40)$$

$$\begin{split} &D\hat{G}(\hat{G}(\boldsymbol{\Phi}_{2},X_{2}),X_{2}) + D\mu\hat{G}(\hat{G}(\boldsymbol{\Phi}_{1},X_{1}),X_{2}) \\ &+ \frac{Sh^{3}}{12} \left(\hat{G}(\hat{G}(\boldsymbol{\Phi}_{2},X_{1}),X_{1}) + \hat{G}(\hat{G}(\boldsymbol{\Phi}_{1},X_{2}),X_{1}) \right) - k_{s}Sh \left(\hat{G}(u_{3},X_{2}) + \boldsymbol{\Phi}_{2} \right) = 0 \end{split} \tag{41}$$

$$k_{s}Sh(\hat{G}(\hat{G}(u_{3},X_{1}),X_{1}) + \hat{G}(\boldsymbol{\Phi}_{1},X_{1})) + k_{s}Sh(\hat{G}(\hat{G}(u_{3},X_{2}),X_{2}) + \hat{G}(\boldsymbol{\Phi}_{2},X_{2})) + \theta_{1}\hat{G}(\hat{G}(u_{3},X_{1}),X_{1}) + \theta_{2}\hat{G}(\hat{G}(u_{3},X_{2}),X_{2}) - q = 0$$

$$(42)$$

Equations 40 and 41 may be written as:

$$\begin{split} D\hat{G}(\hat{G}(\hat{G}(\hat{G}(\boldsymbol{\Phi}_{1},X_{1}),X_{1}),X_{1}) + D\mu\hat{G}(\hat{G}(\hat{G}(\boldsymbol{\Phi}_{2},X_{1}),X_{2}),X_{1}) & + \frac{Sh^{3}}{12} \left(\hat{G}(\hat{G}(\hat{G}(\boldsymbol{\Phi}_{2},X_{1}),X_{1}),X_{2}) + \hat{G}(\hat{G}(\hat{G}(\boldsymbol{\Phi}_{1},X_{2}),X_{1}),X_{2}) \right) \\ & + \frac{Sh^{3}}{12} \left(\hat{G}(\hat{G}(\hat{G}(\boldsymbol{\Phi}_{1},X_{2}),X_{2}),X_{1}) + \hat{G}(\hat{G}(\hat{G}(\boldsymbol{\Phi}_{2},X_{2}),X_{1}),X_{1}) \right) \\ & - k_{s}Sh \left(\hat{G}(\hat{G}(u_{3},X_{2}),X_{2}) + \hat{G}(\boldsymbol{\Phi}_{2},X_{2}) \right) = 0 \\ & - k_{s}Sh \left(\hat{G}(\hat{G}(u_{3},X_{1}),X_{1}) + \hat{G}(\boldsymbol{\Phi}_{1},X_{1}) \right) = 0 \end{split}$$

$$(44) \quad \text{Upon adding the Eqs. 43 and 44, we get:}$$

Upon adding the Eqs. 43 and 44, we get:

 $D\hat{G}(\hat{G}(\hat{G}(\Phi_2, X_2), X_2), X_2) + D\mu\hat{G}(\hat{G}(\hat{G}(\Phi_1, X_1), X_2), X_2)$

$$D\hat{G}(\hat{G}(\hat{G}(\Phi_{1}, X_{1}), X_{1}), X_{1}) + D\hat{G}(\hat{G}(\hat{G}(\Phi_{2}, X_{2}), X_{2}), X_{2})$$

$$D\hat{G}(\hat{G}(\hat{G}(\Phi_{1}, X_{1}), X_{2}), X_{2}) \left(\mu + \frac{2Sh^{3}}{12D}\right) + D\hat{G}(\hat{G}(\hat{G}(\Phi_{2}, X_{1}), X_{1}), X_{2}) \left(\mu + \frac{2Sh^{3}}{12D}\right)$$

$$-k_{s}Sh(\hat{G}(\hat{G}(u_{3}, X_{1}), X_{1}) + \hat{G}(\Phi_{1}, X_{1})) - k_{s}Sh(\hat{G}(\hat{G}(u_{3}, X_{2}), X_{2}) + \hat{G}(\Phi_{2}, X_{2})) = 0$$

$$(45)$$

Using the fact that, $\left(\mu + \frac{2Sh^3}{12D}\right) = 1$, the above Eqn takes the form:

$$\begin{split} D\hat{G}(\hat{G}(\hat{G}(\hat{G}(\boldsymbol{\Phi}_{1},X_{1}),X_{1}),X_{1}) + D\hat{G}(\hat{G}(\hat{G}(\boldsymbol{\Phi}_{2},X_{2}),X_{2}),X_{2}) \\ D\hat{G}(\hat{G}(\hat{G}(\boldsymbol{\Phi}_{1},X_{1}),X_{2}),X_{2}) + D\hat{G}(\hat{G}(\hat{G}(\boldsymbol{\Phi}_{2},X_{1}),X_{1}),X_{2}) \\ -k_{s}Sh(\hat{G}(\hat{G}(u_{3},X_{1}),X_{1}) + \hat{G}(\boldsymbol{\Phi}_{1},X_{1})) - k_{s}Sh(\hat{G}(\hat{G}(u_{3},X_{2}),X_{2}) + \hat{G}(\boldsymbol{\Phi}_{2},X_{2})) = 0 \end{split} \tag{46}$$



However, Eq. 42 may be rewritten as:

$$k_{s}Sh(\hat{G}(\hat{G}(\hat{G}(\hat{G}(u_{3},X_{1}),X_{1}),X_{1}),X_{1}) + \hat{G}(\hat{G}(\hat{G}(\boldsymbol{\Phi}_{1},X_{1}),X_{1}),X_{1})) + k_{s}Sh(\hat{G}(\hat{G}(\hat{G}(u_{3},X_{2}),X_{2}),X_{1}),X_{1}) + \hat{G}(\hat{G}(\hat{G}(\boldsymbol{\Phi}_{2},X_{2}),X_{1}),X_{1})) + \vartheta_{1}\hat{G}(\hat{G}(\hat{G}(\hat{G}(u_{3},X_{1}),X_{1}),X_{1}) + \vartheta_{2}\hat{G}(\hat{G}(\hat{G}(\hat{G}(u_{3},X_{2}),X_{2}),X_{1}),X_{1}) - \hat{G}(\hat{G}(q,X_{1}),X_{1}) = 0$$

$$(47)$$

and,

$$k_{s}Sh(\hat{G}(\hat{G}(\hat{G}(\hat{G}(u_{3},X_{1}),X_{1}),X_{2}),X_{2}) + \hat{G}(\hat{G}(\hat{G}(\boldsymbol{\Phi}_{1},X_{1}),X_{2}),X_{2}))$$

$$+k_{s}Sh(\hat{G}(\hat{G}(\hat{G}(\hat{G}(u_{3},X_{2}),X_{2}),X_{2}),X_{2}) + \hat{G}(\hat{G}(\hat{G}(\boldsymbol{\Phi}_{2},X_{2}),X_{2}),X_{2}))$$

$$+\vartheta_{1}\hat{G}(\hat{G}(\hat{G}(\hat{G}(u_{3},X_{1}),X_{1}),X_{2}),X_{2}) + \vartheta_{2}\hat{G}(\hat{G}(\hat{G}(\hat{G}(u_{3},X_{2}),X_{2}),X_{2}),X_{2})$$

$$-\hat{G}(\hat{G}(q,X_{2}),X_{2}) = 0$$

$$(48)$$

Adding the Eqs. 47 and 48, we get:

$$\begin{aligned} k_s \mathcal{S}h \Big(\hat{G}(\hat{G}(\hat{G}(\hat{G}(G_{3},X_{1}),X_{1}),X_{1}),X_{1}) + \hat{G}(\hat{G}(\hat{G}(\Phi_{1},X_{1}),X_{1}),X_{1}) \Big) \\ + k_s \mathcal{S}h \Big(\hat{G}(\hat{G}(\hat{G}(G_{3},X_{1}),X_{1}),X_{1}),X_{1}) + \hat{G}(\hat{G}(\hat{G}(\Phi_{1},X_{1}),X_{2}),X_{2}) \Big) \\ + k_s \mathcal{S}h \Big(\hat{G}(\hat{G}(\hat{G}(G_{3},X_{2}),X_{2}),X_{1}),X_{1}) + \hat{G}(\hat{G}(\hat{G}(\Phi_{2},X_{2}),X_{1}),X_{1}) \Big) \\ + \vartheta_{1} \hat{G}(\hat{G}(\hat{G}(\hat{G}(G_{3},X_{1}),X_{1}),X_{1}),X_{1}) + \vartheta_{2} \hat{G}(\hat{G}(\hat{G}(G_{3},X_{2}),X_{2}),X_{1}),X_{1}) \\ - \hat{G}(\hat{G}(q,X_{1}),X_{1}) \\ + k_s \mathcal{S}h \Big(\hat{G}(\hat{G}(\hat{G}(G_{3},X_{2}),X_{2}),X_{1}),X_{1}) + \hat{G}(\hat{G}(\hat{G}(\Phi_{2},X_{2}),X_{1}),X_{1}) \Big) \\ + \vartheta_{1} \hat{G}(\hat{G}(\hat{G}(G_{3},X_{1}),X_{1}),X_{1}) + \vartheta_{2} \hat{G}(\hat{G}(\hat{G}(G_{3},X_{2}),X_{2}),X_{1}),X_{1}) \\ - \hat{G}(\hat{G}(q,X_{1}),X_{1}) = 0 \end{aligned} \tag{49}$$

Substituting Eqs. 44 in Eq. 49 and rearranging the terms leads to:

$$\begin{split} &D\big(\hat{G}(\hat{G}(\hat{G}(\hat{G}(\hat{G}(u_3,X_1),X_1),X_1),X_1) + 2\hat{G}(\hat{G}(\hat{G}(\hat{G}(u_3,X_1),X_1),X_2),X_2) \\ &+ \hat{G}(\hat{G}(\hat{G}(\hat{G}(u_3,X_2),X_2),X_2),X_2)\big) \\ &+ \vartheta_1 \left(\frac{D}{k_s Sh} \Big(\hat{G}(\hat{G}(\hat{G}(\hat{G}(u_3,X_1),X_1),X_1),X_1) \\ &+ \hat{G}(\hat{G}(\hat{G}(\hat{G}(\hat{G}(u_3,X_1),X_1),X_2),X_2) \Big) + \hat{G}(\hat{G}(u_3,X_1),X_1) \Big) \\ &+ \vartheta_2 \left(\frac{D}{k_s Sh} \Big(\hat{G}(\hat{G}(\hat{G}(\hat{G}(u_3,X_2),X_2),X_2),X_2) + \hat{G}(\hat{G}(\hat{G}(\hat{G}(u_3,X_1),X_1),X_2),X_2) \Big) \\ &+ \hat{G}(\hat{G}(u_3,X_2),X_2) \Big) \\ &- q - \frac{D}{k_s Sh} \Big(\hat{G}(\hat{G}(q,X_1),X_1) + \hat{G}(\hat{G}(q,X_2),X_2) \Big) = 0 \end{split}$$



With the assumption that for a shear rigid (Kirchhoff) plate:

$$\frac{D}{k_s Sh} << 1 \tag{51}$$

we arrive at the governing equation for a shear rigid plate in the static case.

$$\left[\int_{X_1 - r_c}^{X_1 + r_c} (Y_1 - \overline{Y}_1) (Y_1 - \overline{Y}_1)^T dY_1 \right] = \frac{2r_c^3}{3}
\left[\int_{X_2 - r_c}^{X_2 + r_c} (Y_2 - \overline{Y}_2) (Y_2 - \overline{Y}_2)^T dY_2 \right] = \frac{2r_c^3}{3}$$
(56)

Substitution of Eq. (56) in the Eq. (55) yields:

$$D(\hat{G}(\hat{G}(\hat{G}(\hat{G}(u_3, X_1), X_1), X_1), X_1) + 2\hat{G}(\hat{G}(\hat{G}(\hat{G}(u_3, X_1), X_1), X_2), X_2)$$

$$+\hat{G}(\hat{G}(\hat{G}(\hat{G}(u_3, X_2), X_2), X_2), X_2))$$

$$+\vartheta_1(\hat{G}(\hat{G}(u_3, X_1), X_1)) + \vartheta_2(\hat{G}(\hat{G}(u_3, X_2), X_2)) - q = 0$$
(52)

Therefore, with the assumption that $\frac{D}{k_s Sh} \ll 1$, the shear deformable plate theory becomes equivalent to shear-rigid (Kirchhoff) plate theory for a thin plate.

$$\hat{G}(\xi, X_1) = -C_1 \xi^0 \cos(\alpha X_1) \sin(\beta X_2) \hat{G}(\xi, X_2) = -C_2 \xi^0 \sin(\alpha X_1) \cos(\beta X_2)$$
(57)

where,

Appendix 4: Computation of analytical expressions for
$$\hat{G}(\hat{G}(\xi, X_d), X_d)$$

Let us assume a field variable ξ defined by the far-off interactions of any material point X such that,

$$\xi = \xi^0 \sin(\alpha X_1) \sin(\beta X_2) \tag{53}$$

The derivative-free directionality term $\hat{G}(\xi, X_1)$ and $\hat{G}(\xi, X_2)$ can be computed as:

$$C_1 = \frac{3}{\alpha^2 r_c^3} (\alpha r_c \cos(\alpha r_c) - \sin(\alpha r_c))$$

$$C_2 = \frac{3}{\beta^2 r_c^3} (\beta r_c \cos(\beta r_c) - \sin(\beta r_c))$$
(58)

The expression for $\hat{G}(\hat{G}(\xi, X_1), X_1)$ can be computed as:

$$\hat{G}(\xi, X_1) = \left[\int_{\Omega_X} (\xi - \overline{\xi})((Y_1 - \overline{Y}_1)^T dY_1 \right] \left[\int_{\Omega_X} (Y_1 - \overline{Y}_1)((Y_1 - \overline{Y}_1)^T dY_1 \right]^{-1}$$

$$\hat{G}(\xi, X_2) = \left[\int_{\Omega_X} (\xi - \overline{\xi})((Y_2 - \overline{Y}_2)^T dY_2 \right] \left[\int_{\Omega_X} (Y_2 - \overline{Y}_2)(Y_2 - \overline{Y}_2)^T dY_2 \right]^{-1}$$
(54)

For an influence domain of definite length r_c , the above expressions take the form,

$$\hat{G}(\xi, X_{1}) = \left[\int_{X_{1} - r_{c}}^{X_{1} + r_{c}} (\xi - \overline{\xi}) (Y_{1} - \overline{Y}_{1})^{T} dY_{1} \right] \left[\int_{X_{1} - r_{c}}^{X_{1} + r_{c}} (Y_{1} - \overline{Y}_{1}) (Y_{1} - \overline{Y}_{1})^{T} dY_{1} \right]^{-1} \\
\hat{G}(\xi, X_{2}) = \left[\int_{X_{2} - r_{c}}^{X_{2} + r_{c}} (\xi - \overline{\xi}) (Y_{2} - \overline{Y}_{2})^{T} dY_{2} \right] \left[\int_{X_{2} - r_{c}}^{X_{2} + r_{c}} (Y_{2} - \overline{Y}_{2})^{T} dY_{2} \right]^{-1}$$
(55)

where,



$$\hat{G}(\hat{G}(\xi, X_1), X_1) = \left[\int_{X_1 - r_c}^{X_1 + r_c} (\hat{G}(\xi, X_1) - \overline{\hat{G}(\xi, X_1)}) (Y_1 - \overline{Y}_1)^T dY_1 \right] \frac{3}{2rc^3}$$

$$= C_1^2 \xi^0 \sin(\alpha X_1) \sin(\beta X_2)$$
(59)

Similarly,

$$\hat{G}(\hat{G}(\xi, X_2), X_2) = \left[\int_{X_2 - r_c}^{X_2 + r_c} (\hat{G}(\xi, X_2) - \overline{\hat{G}(\xi, X_2)}) (Y_2 - \overline{Y}_2)^T dY_2 \right] \frac{3}{2rc^3}$$

$$= C_2^2 \xi^0 \sin(\alpha X_1) \sin(\beta X_2)$$
(60)

and,

$$\hat{G}(\hat{G}(\xi, X_1), X_2) = \left[\int_{X_2 - r_c}^{X_2 + r_c} (\hat{G}(\xi, X_1) - \overline{\hat{G}(\xi, X_1)}) (Y_2 - \overline{Y}_2)^T dY_2 \right] \frac{3}{2rc^3}$$

$$= C_1 C_2 \xi^0 \sin(\alpha X_1) \sin(\beta X_2)$$
(61)

References

- Maleki-Bigdeli MA, Sheikhi S, Baghani M (2021) Development of an analytical framework for viscoelastic corrugated-core sandwich plates and validation against fem. Meccanica 56:2103–2120
- Wollmann L, Nayak AK, Parkin SSP, Felser C (2017) Heusler 4.0: tunable materials. Annu Rev Mater Res 47(1):247–270
- Vigliotti A, Pasini D (2012) Stiffness and strength of tridimensional periodic lattices. Comput Methods Appl Mech Eng 229:27–43
- Fleck N, Deshpande V, Ashby M (2010) Micro-architectured materials: past, present and future. Proc R Soc Lond Math Phys Eng Sci 466:2495–2516
- Kolsters H, Zenkert D (2010) Buckling of laser-welded sandwich panels: ultimate strength and experiments. Proc Inst Mech Eng Part M J Eng Marit Environ 224(1):29–45
- Jelovica J, Romanoff J, Ehlers S, Aromaa J (2013) Ultimate strength of corroded web-core sandwich beams. Mar Struct 31:1–14
- Jiang XX, Zhu L, Qiao JS, Wu YX, Li ZG, Chen JH (2014) The strength of laser welded web-core steel sandwich plates. In: Applied mechanics and materials vol 551, Trans Tech Publ, pp 42–46
- Bright S, Smith J (2007) A new design for steel bridge decks using laser fabrication. Struct Eng 85(21):49–57
- Nilsson P, Al-Emrani M, Atashipour SR (2017) Transverse shear stiffness of corrugated core steel sandwich panels with dual weld lines. Thin-walled Struct 117:98–112
- Briscoe CR, Mantell SC, Davidson JH, Okazaki T (2011) Design procedure for web core sandwich panels for residential roofs. J Sandw Struct Mater 13(1):23–58

- Bapanapalli S, Martinez O, Gogu C, Sankar B, Haftka R, Blosser M (2006) Analysis and design of corrugatedcore sandwich panels for thermal protection systems of space vehicles. In: 47th AIAA/ASME/ASCE/AHS/ASC structures, structural dynamics, and materials conference 14th AIAA/ASME/ahs adaptive structures conference 7th, p 1942
- 12. Bright S, Smith J (2004) Fatigue performance of laser-welded steel bridge decks. Struct Eng 82(21):31
- Sharma A, Sankar B, Haftka R (2010) Homogenization of plates with microstructure and application to corrugated core sandwich panels. In: 51st AIAA/ASME/ ASCE/AHS/ASC structures, structural dynamics, and materials conference 18th AIAA/ASME/AHS adaptive structures conference 12th, p 2706
- Reddy J (2007) Nonlocal theories for bending, buckling and vibration of beams. Int J Eng Sci 45(2–8):288–307
- Lim CW, Zhang G, Reddy JN (2015) A higher-order nonlocal elasticity and strain gradient theory and its applications in wave propagation. J Mech Phys Solids 78:298–313
- Cosserat E, Cosserat F (1909) Theories des corps deformables, A. Hermann et fils
- Eringen AC, Wegner J (2003) Nonlocal continuum field theories. Appl Mech Rev 56(2):B20–B22
- Yang F, Chong A, Lam DCC, Tong P (2002) Couple stress based strain gradient theory for elasticity. Int J Solids Struct 39(10):2731–2743
- Akgöz B, Civalek Ö (2013) Modeling and analysis of micro-sized plates resting on elastic medium using the modified couple stress theory. Meccanica 48:863–873
- Ma H, Gao XL, Reddy JN (2008) A microstructure-dependent Timoshenko beam model based on a modified couple stress theory. J Mech Phys Solids 56(12):3379–3391



- Reddy JN (2011) Microstructure-dependent couple stress theories of functionally graded beams. J Mech Phys Solids 59(11):2382–2399
- 22. Romano G, Diaco M (2021) On formulation of nonlocal elasticity problems. Meccanica 56(6):1303–1328
- 23. Demir C, Civalek Ö (2017) On the analysis of microbeams. Int J Eng Sci 121:14–33
- Akgöz B, Civalek Ö (2022) Buckling analysis of functionally graded tapered microbeams via Rayleigh-Ritz method. Mathematics 10(23):4429
- Jalaei M, Thai H, Civalek O (2022) On viscoelastic transient response of magnetically imperfect functionally graded nanobeams. Int J Eng Sci 172:103629
- Aghababaei R, Reddy JN (2009) Nonlocal third-order shear deformation plate theory with application to bending and vibration of plates. J Sound Vib 326(1–2):277–289
- Lu P, Zhang P, Lee H, Wang C, Reddy JN (2007) Nonlocal elastic plate theories. Proc R Soc Math Phys Eng Sci 463(2088):3225–3240
- Srividhya S, Raghu P, Rajagopal A, Reddy JN (2018) Nonlocal nonlinear analysis of functionally graded plates using third-order shear deformation theory. Int J Eng Sci 125:1–22
- Romanoff J, Reddy JN, Jelovica J (2016) Using nonlocal Timoshenko beam theories for prediction of micro-and macro-structural responses. Compos Struct 156:410–420
- Karttunen AT, Reddy JN, Romanoff J (2018) Micropolar modeling approach for periodic sandwich beams. Compos Struct 185:656–664
- Karttunen AT, Reddy JN, Romanoff J (2019) Two-scale micropolar plate model for web-core sandwich panels. Int J Solids Struct 170:82–94
- 32. Faghidian SA, Ghavanloo E (2021) Unified higher-order theory of two-phase nonlocal gradient elasticity. Meccanica 56(3):607–627
- Saxena M, Sarkar S, Roy D (2022) A microstructure-sensitive and derivative-free continuum model for composite materials: applications to concrete. Int J Solids Struct 262:112051
- Sarkar S, Roy D, Vasu RM (2015) A global optimization paradigm based on change of measures. R Soc Open Sci 2(7):150123
- Sarkar S, Chowdhury S, Venugopal M, Vasu R, Roy D (2014) A Kushner–Stratonovich Monte Carlo filter applied to nonlinear dynamical system identification. Phys D 270:46–5904
- Nowruzpour M, Sarkar S, Reddy JN, Roy D (2019) A derivative-free upscaled theory for analysis of defects. J Mech Phys Solids 122:489–501

- 37. Nwoji C, Onah H, Mama B, Ike C (2017) Theory of elasticity formulation of the Mindlin plate equations. Int J Eng Technol (IJET) 9(6):4344–4352
- Srinivasa AR, Reddy JN (2017) An overview of theories of continuum mechanics with nonlocal elastic response and a general framework for conservative and dissipative systems. Appl Mech Rev 10(1115/1):4036723
- Reddy JN (2006) Theory and analysis of elastic plates and shells, 2nd edn. CRC Press, Boca Raton
- Hosseini-Hashemi S, Khorshidi K, Amabili M (2008) Exact solution for linear buckling of rectangular Mindlin plates. J Sound Vib 315(1–2):318–342
- Reddy JN (2003) Mechanics of laminated composite plates and shells: theory and analysis, 2nd edn. CRC Press, Boca Raton
- 42. Bishop G, Welch G (2001) An introduction to the kalman filter. Proc of SIGGRAPH, Course 8(27599–23175), 41
- Kallianpur G (2013) Stochastic filtering theory, vol 13.
 Springer Science & Business Media, New York
- Yang Z, Naumenko K, Ma C-C, Altenbach H, Oterkus E, Oterkus S (2022) Some closed form series solutions to peridynamic plate equations. Mech Res Commun 126:104000
- Yang Z, Naumenko K, Altenbach H, Ma C-C, Oterkus E, Oterkus S (2022) Some analytical solutions to peridynamic beam equations. ZAMM J Appl Math Mech/Z f ür Angew Math Mech 102(10):e202200132
- Yang Z, Naumenko K, Altenbach H, Ma C-C, Oterkus E, Oterkus S (2022) Beam buckling analysis in peridynamic framework. Arch Appl Mech 92(12):3503–3514
- Silling SA, Epton M, Weckner O, Xu J, Askari E (2007) Peridynamic states and constitutive modeling. J Elast 88(2):151–184
- Chen H (2018) Bond-associated deformation gradients for peridynamic correspondence model. Mech Res Commun 90:34–41
- Madenci E, Dorduncu M, Gu X (2019) Peridynamic least squares minimization. Comput Methods Appl Mech Eng 348:846–874

Publisher's Note Springer Nature remains neutral with regard to jurisdictional claims in published maps and institutional affiliations.

Springer Nature or its licensor (e.g. a society or other partner) holds exclusive rights to this article under a publishing agreement with the author(s) or other rightsholder(s); author self-archiving of the accepted manuscript version of this article is solely governed by the terms of such publishing agreement and applicable law.

